Status and future prospect of KAGRA

Takafumi Ushiba on behalf of the KAGRA Collaboration
Institute for Cosmic Ray Research, UTokyo, Japan

Sources of GWs

New eyes to observe the Universe

K. Kokeyama JGW-G1808116

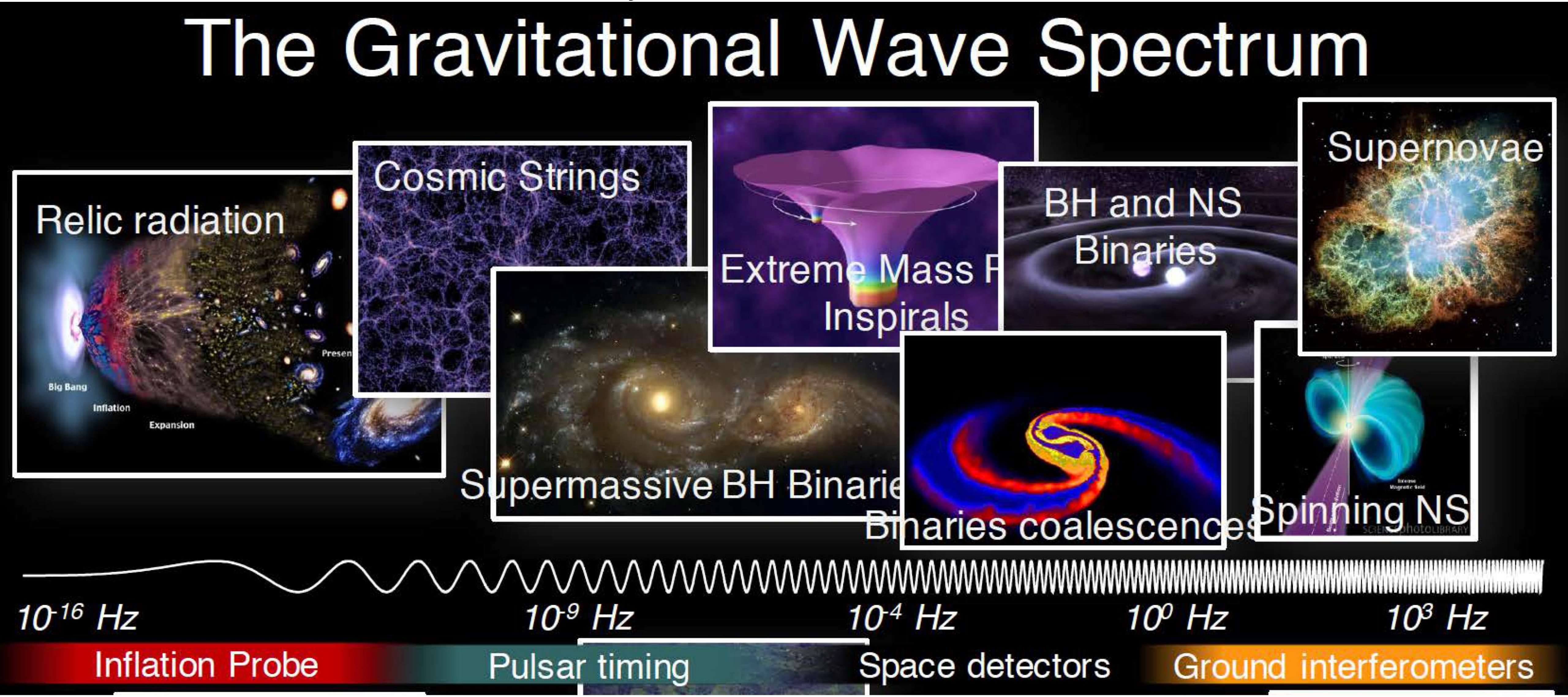

Figure: M Evans

Target of ground-based interferometric GW detectors

Currently GWs above 10 Hz can be detected by LIGO and Virgo. K. Kokeyama JGW-G1808116

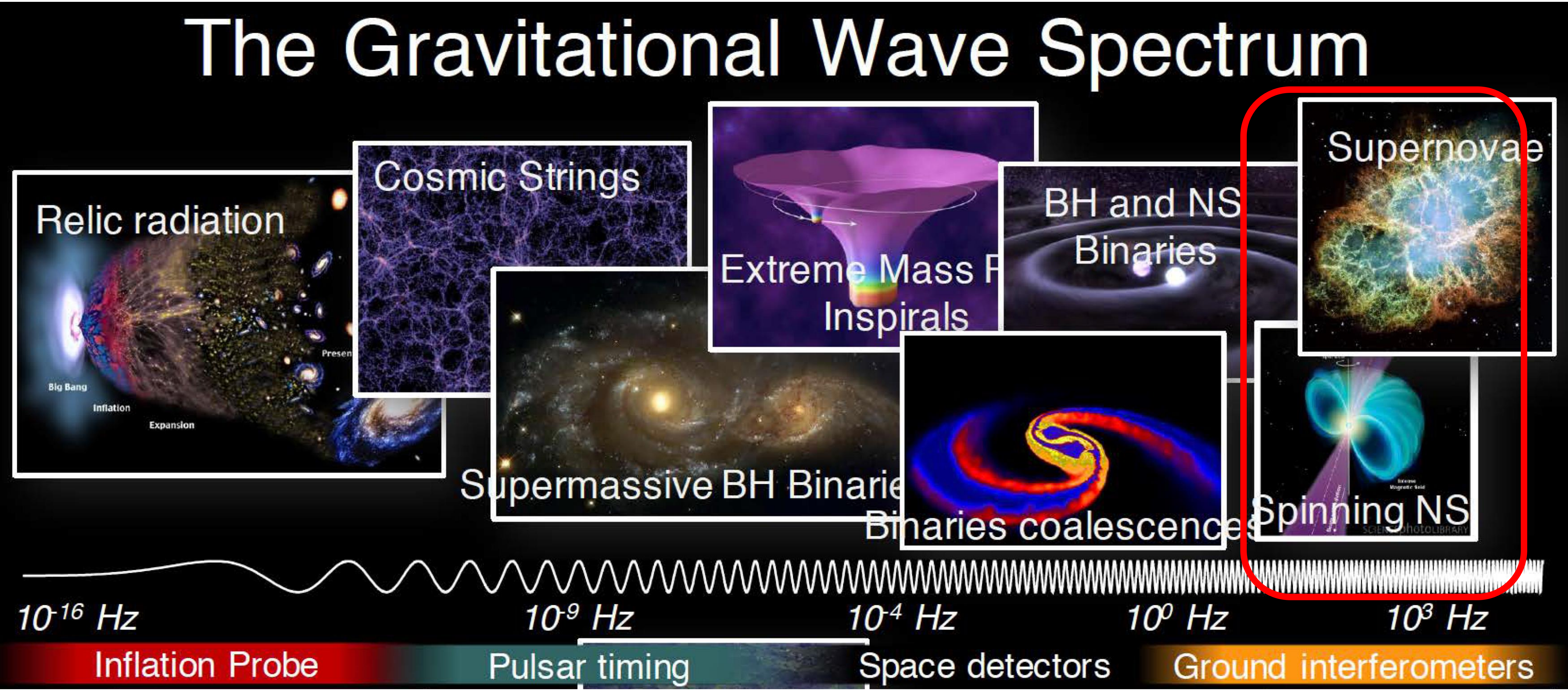

Next generation GWDs and space GWDs will expand the window of GWs

How can we detect GW signals?

Gravitational wave is too faint: strain amplitude of 10^{-21}.

In case we use kilometer-scale detector, we need to detect the displacement of 10^{-18} m

- Achieving to measure such tiny displacement, a laser interferometer based on Michelson interferometer is used.

  Reduce any disturbances causing larger than 10^{-18} m displacement.
  - Seismic noise
  - Thermal noise
  - Radiation pressure noise etc

  Reduce noises accompanying with sensing the displacement.
  - Quantum shot noise
  - PD dark noise
  - ADC noise etc

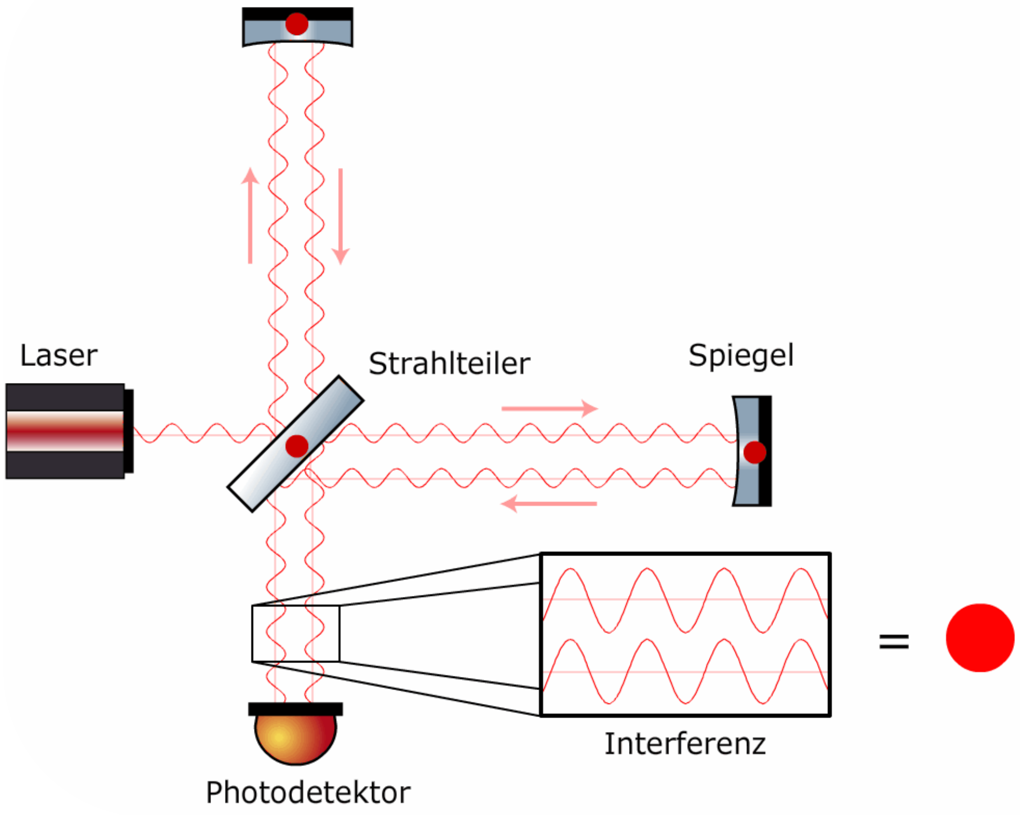

M. Tamaki
JGW-G2214541-v6

How to reduce disturbances?

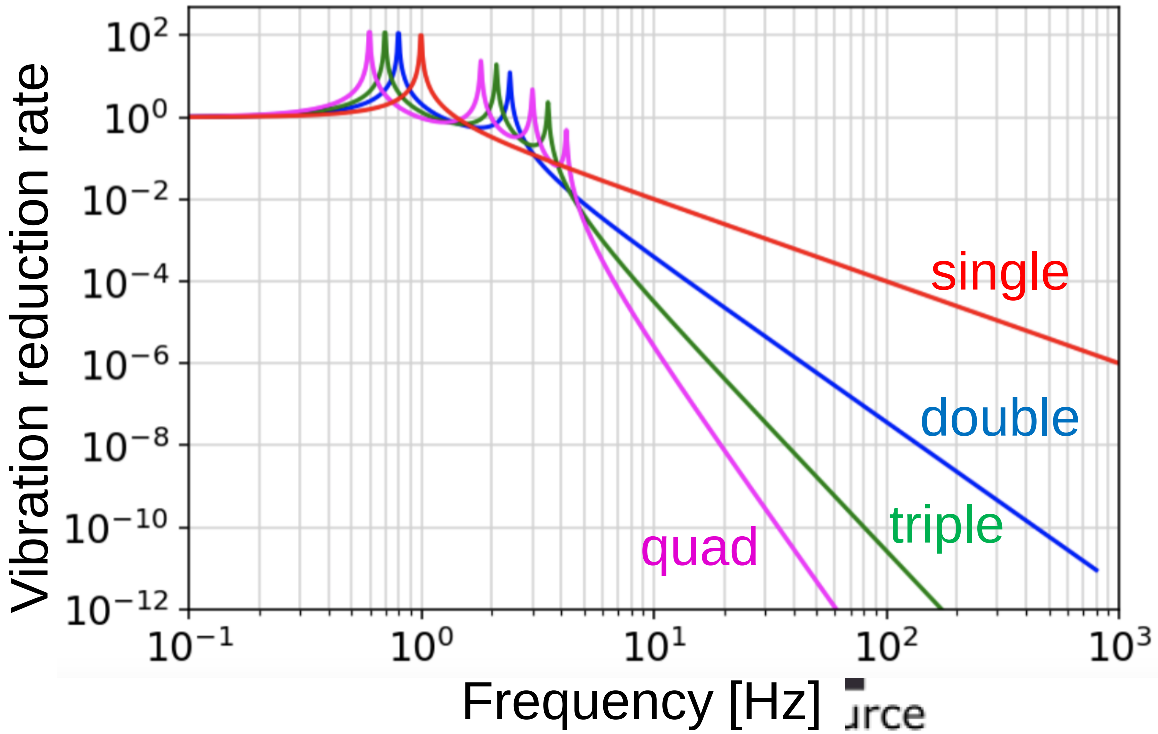

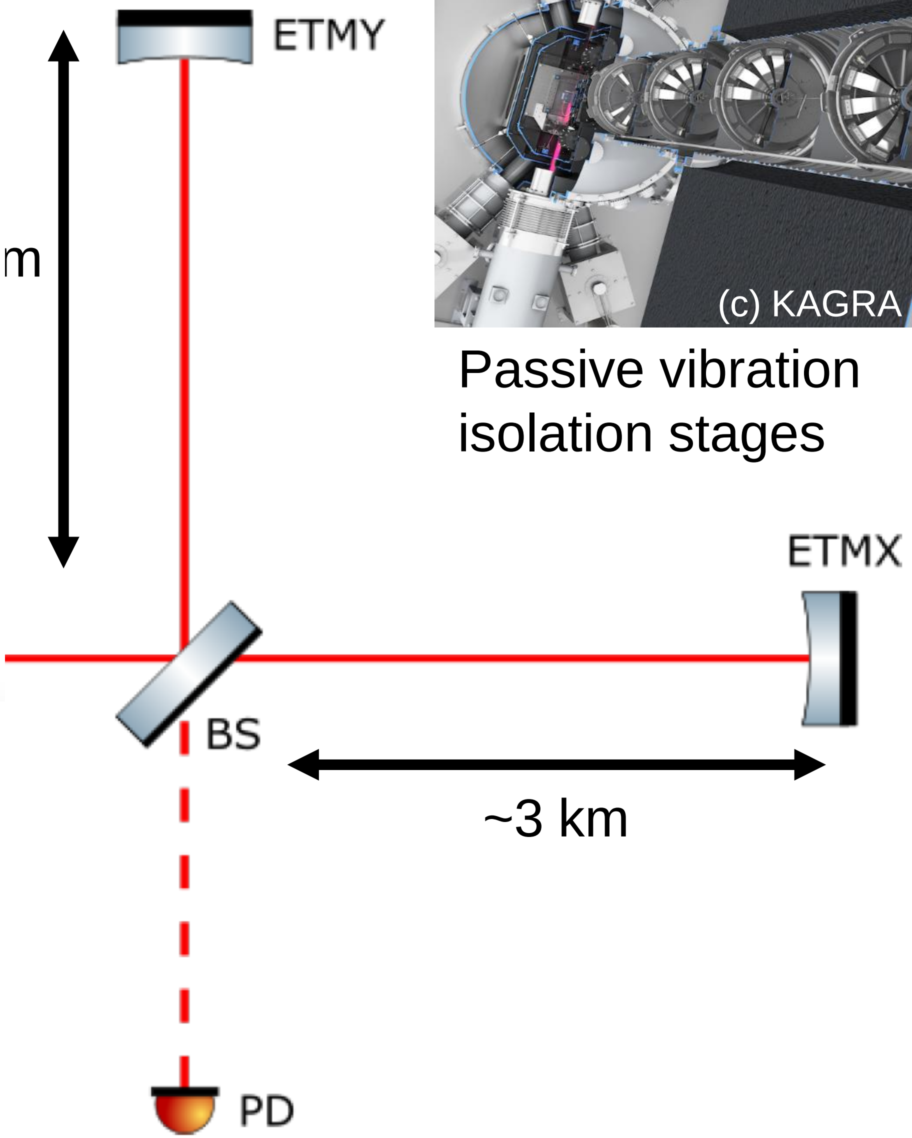

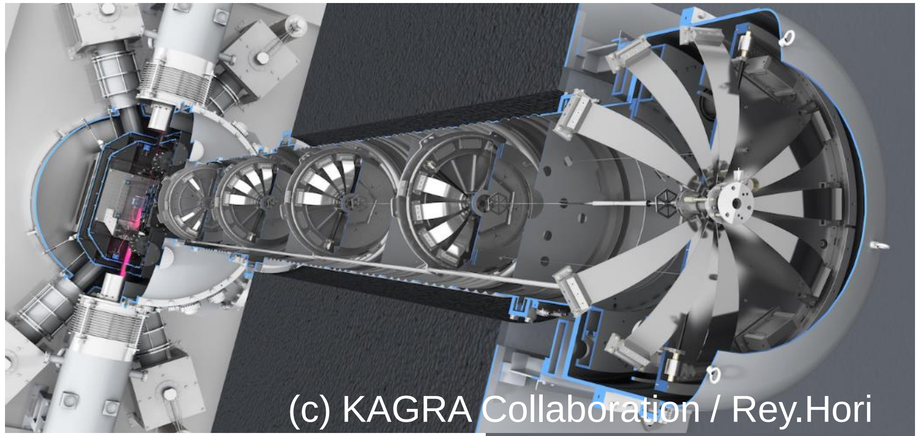

Passive vibration isolation stages

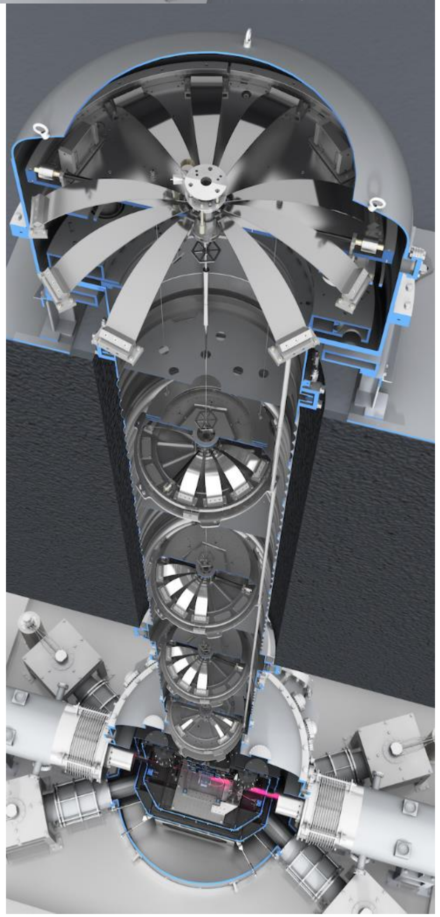

Ground motion ~ 10^{-11} m/rtHz @ 10Hz

7 orders

Target ~ 10^{-18} m/rtHz @ 10Hz

How to reduce disturbances?

Thermal noise:Brownian motions of atoms
Motion of each atom is much larger than our target.

KAGRA case:
Beam size ~ 7cm
Loss angle ~ 10^{-8} (substrate)
Temperature ~ 20K

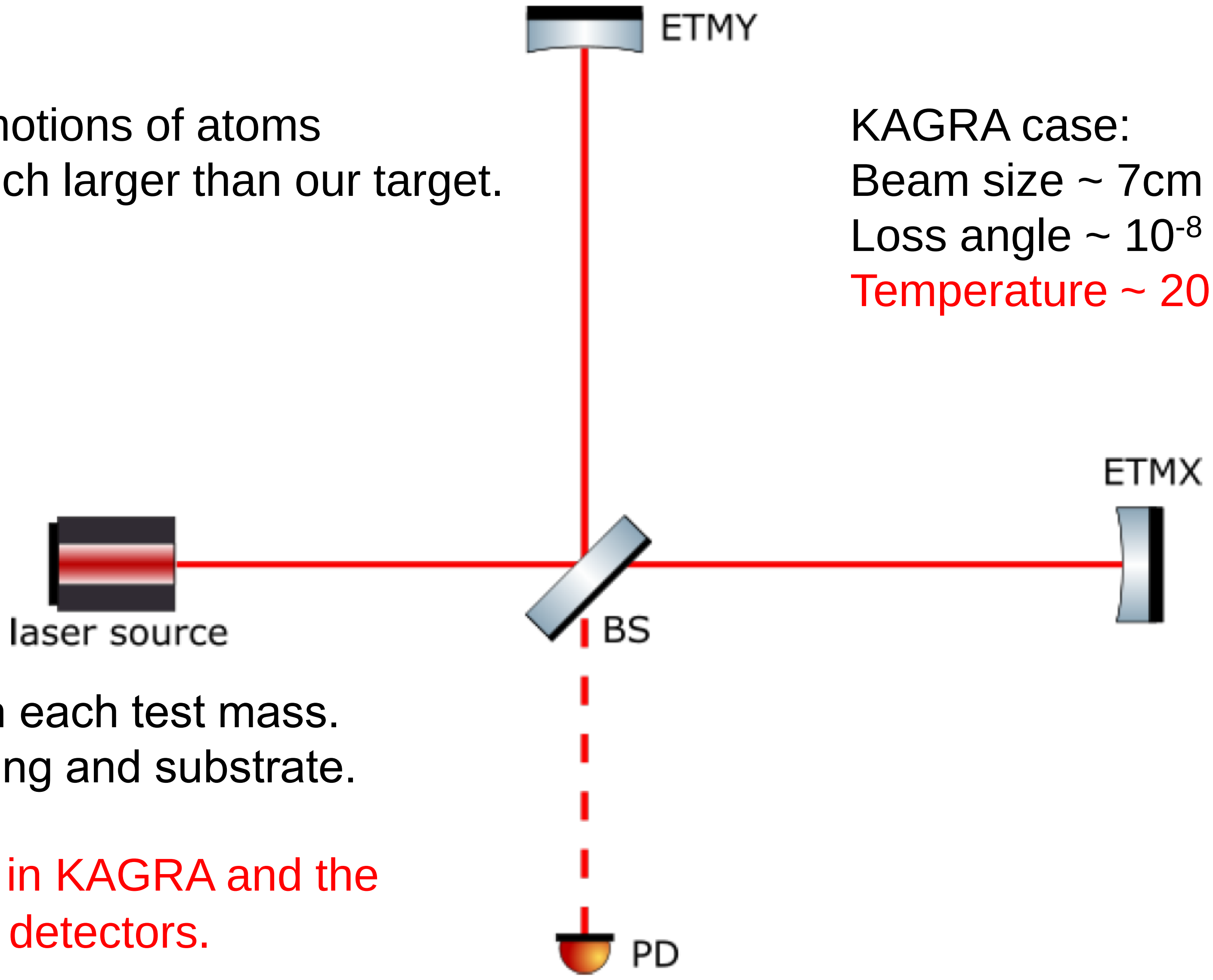

—Enlarge beams on each test mass.
—Use low loss coating and substrate.
—Cooling mirrors.
→ Unique feature in KAGRA and the next generation GW detectors.

How to reduce sensing noise?

Quantum shot noise:
Fluctuation of a number of photons on the photodecter.

- GW signals ∝ laser power
- Shot noise ∝ $\sqrt{\text{laser power}}$

→ Increasing laser power improves S/N.

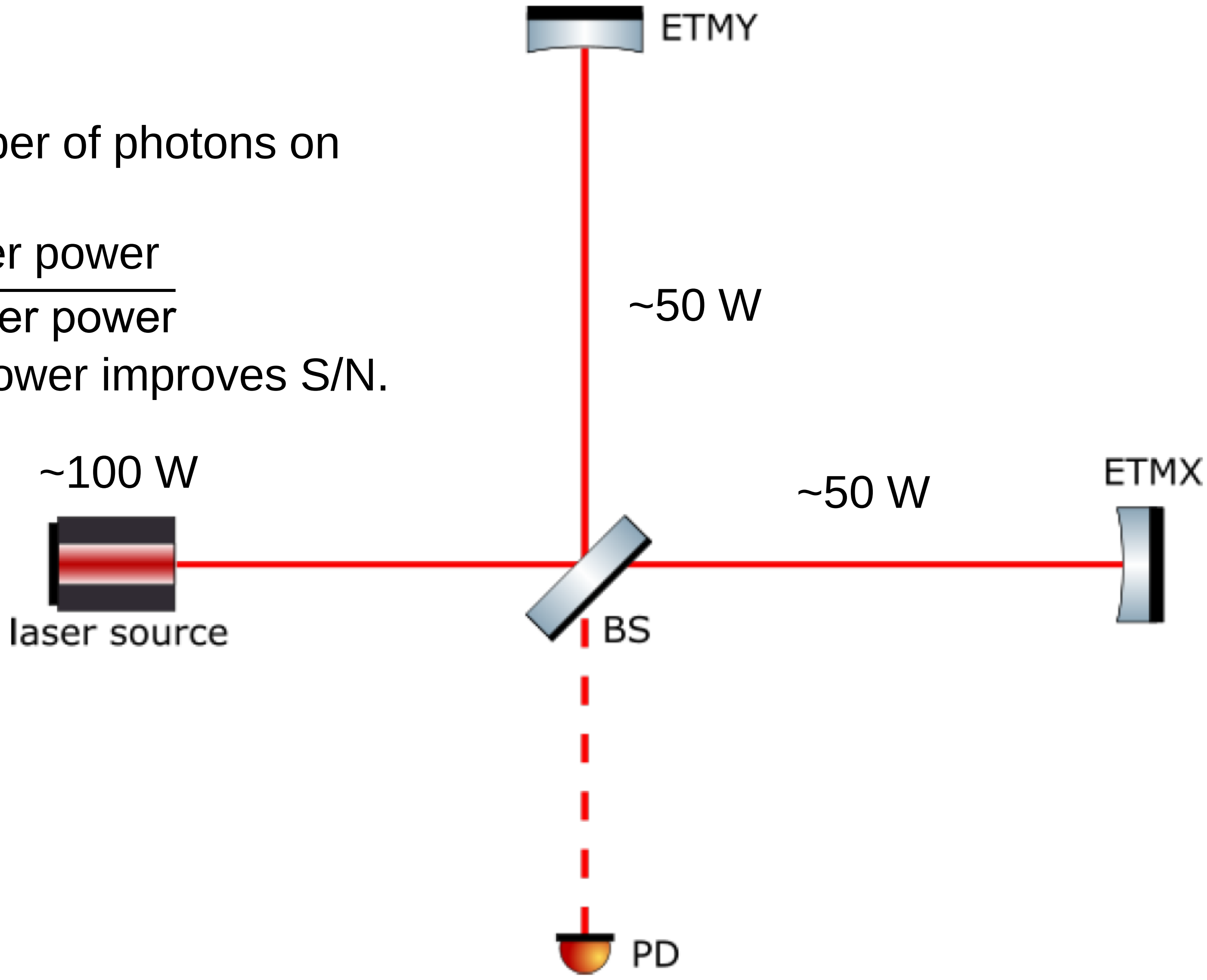

How to reduce sensing noise?

Quantum shot noise:
Fluctuation of a number of photons on the photodecter.

- GW signals $\propto$ laser power
- Shot noise $\propto \sqrt{\text{laser power}}$

$\rightarrow$ Increasing laser power improves S/N.

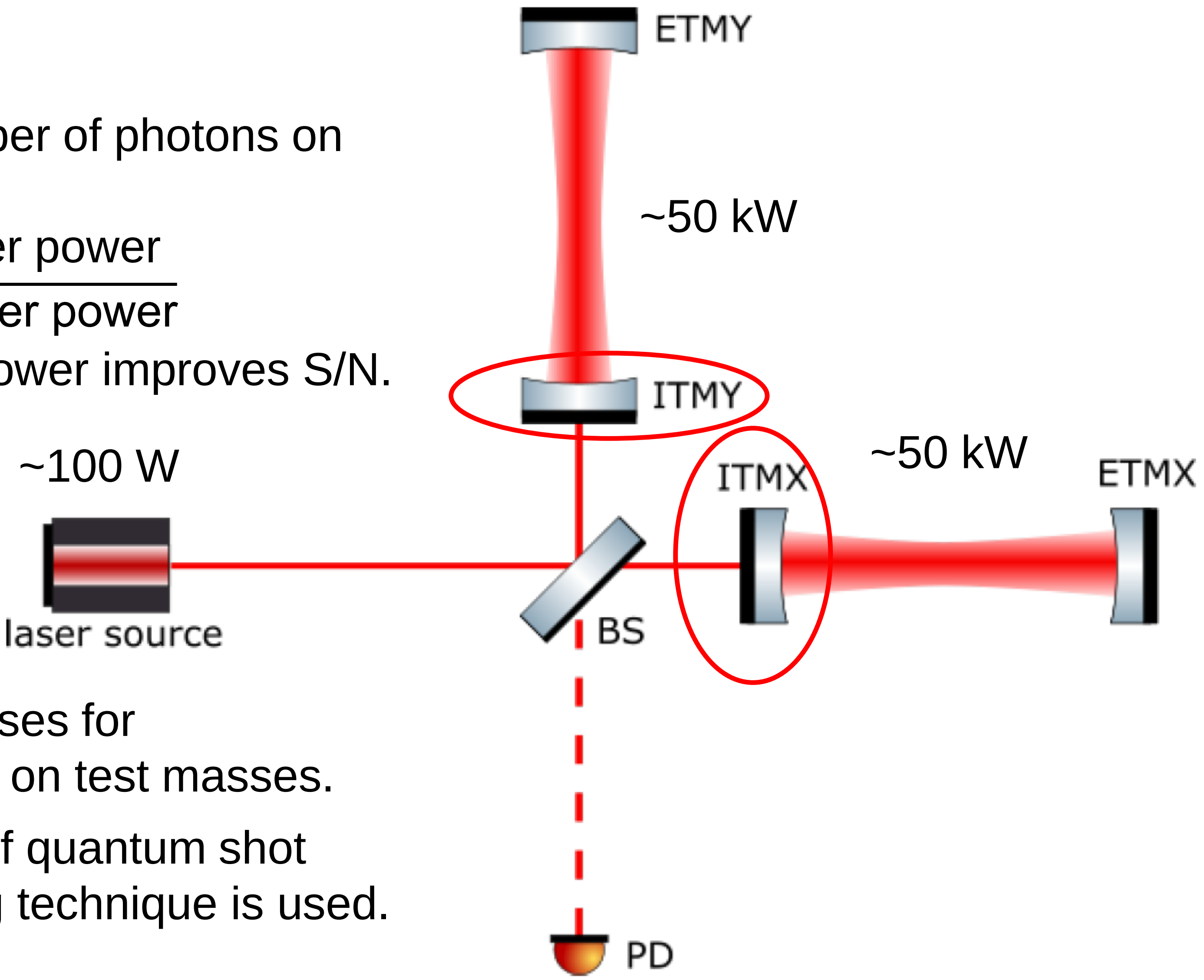

Insert input test masses for increasing the beam on test masses.

For further reduction of quantum shot noise, power-recycling technique is used.

How to reduce sensing noise?

Quantum shot noise:
Fluctuation of a number of photons on the photodecter.

- GW signals $\propto$ laser power
- Shot noise $\propto \sqrt{\text{laser power}}$

→ Increasing laser power improves S/N.

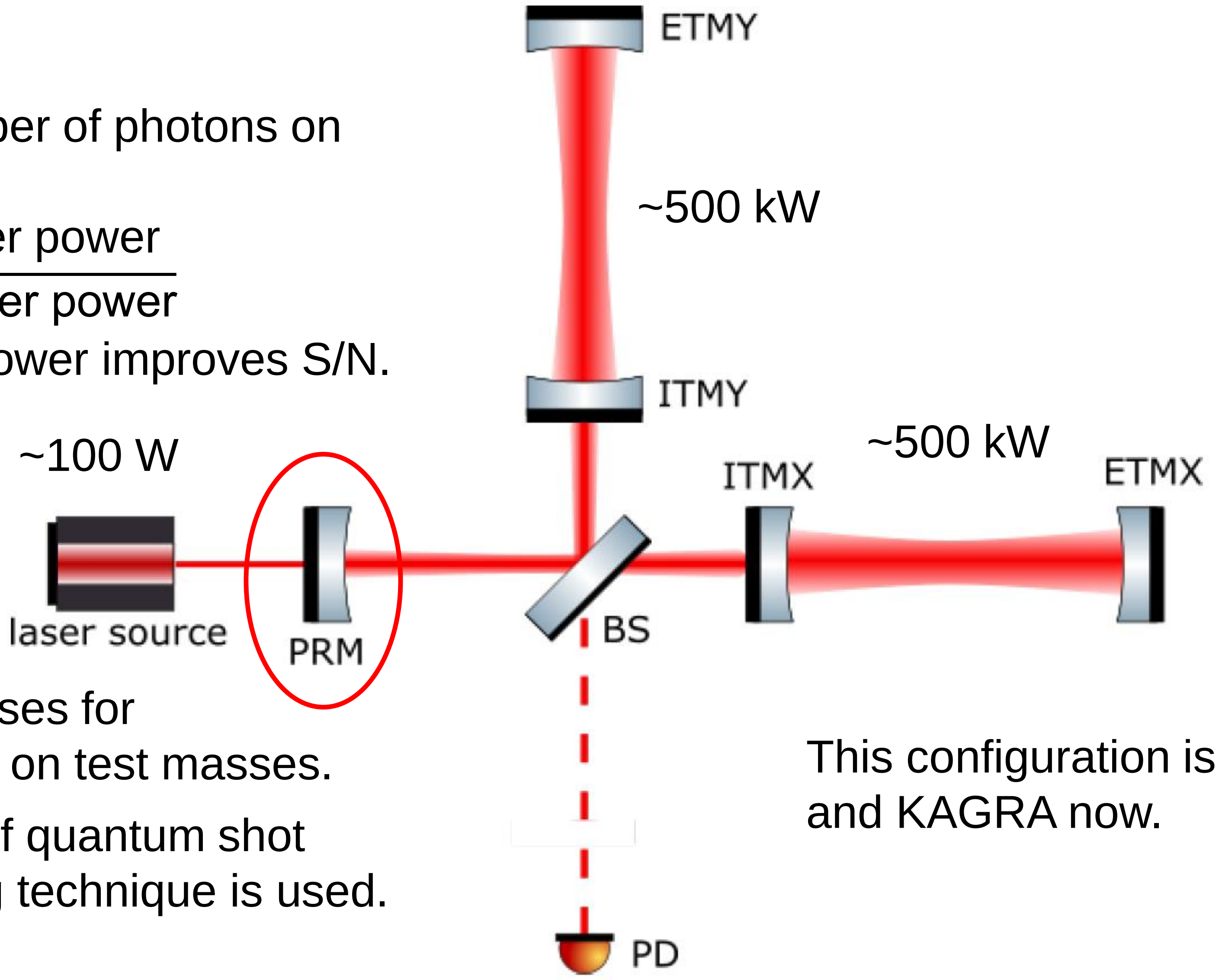

Insert input test masses for increasing the beam on test masses.

For further reduction of quantum shot noise, power-recycling technique is used.

This configuration is used in Virgo and KAGRA now.

How to reduce sensing noise?

Quantum shot noise:
Fluctuation of a number of photons on the photodecter.

- GW signals ∝ laser power
- Shot noise ∝ $\sqrt{\text{laser power}}$

→ Increasing laser power improves S/N.

This configuration is used in current LIGO and will be in future Virgo and KAGRA.

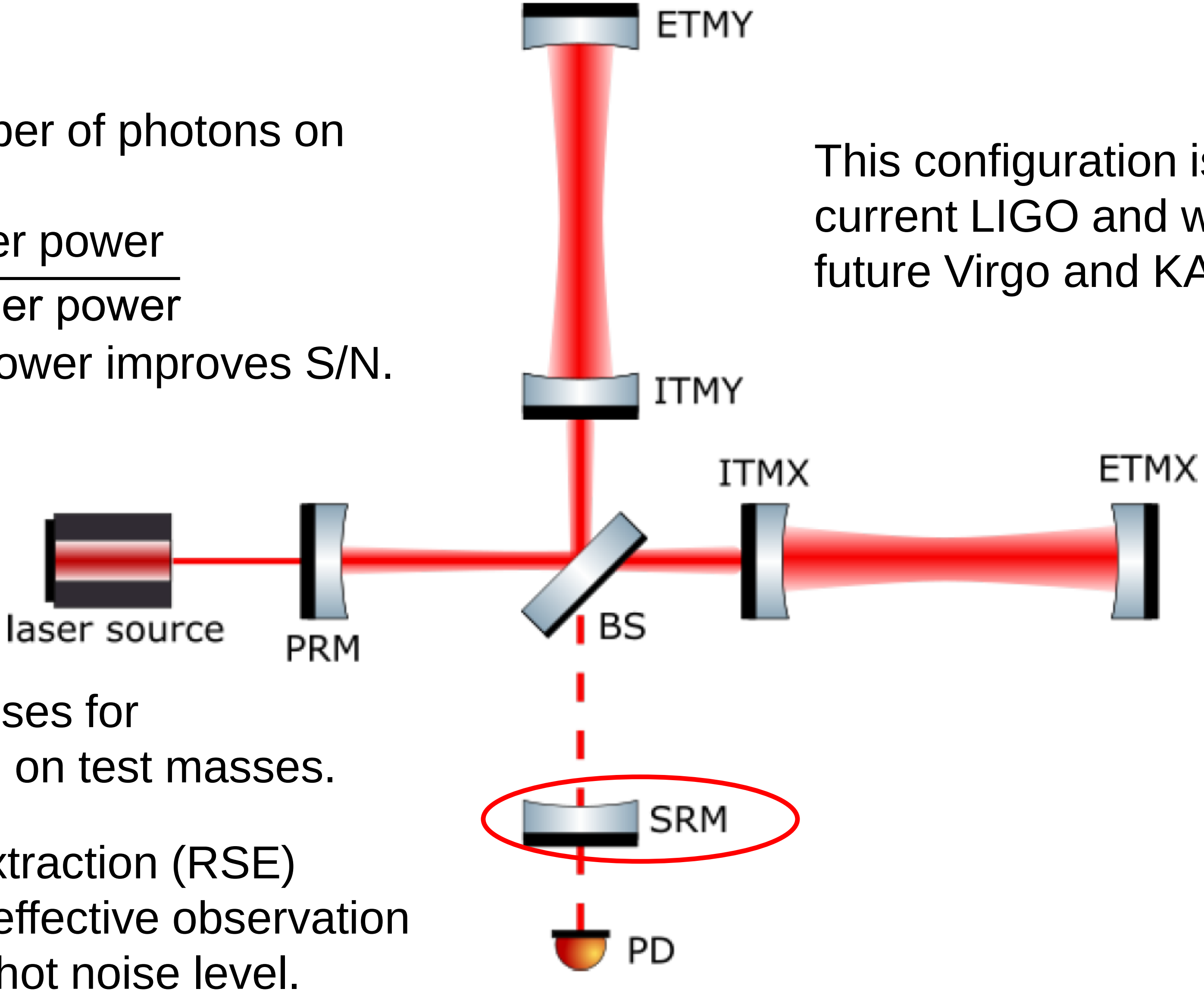

Insert input test masses for increasing the beam on test masses.

Resonant Sideband Extraction (RSE) technique expand the effective observation band and reduce the shot noise level.

Design sensitivity of KAGRA

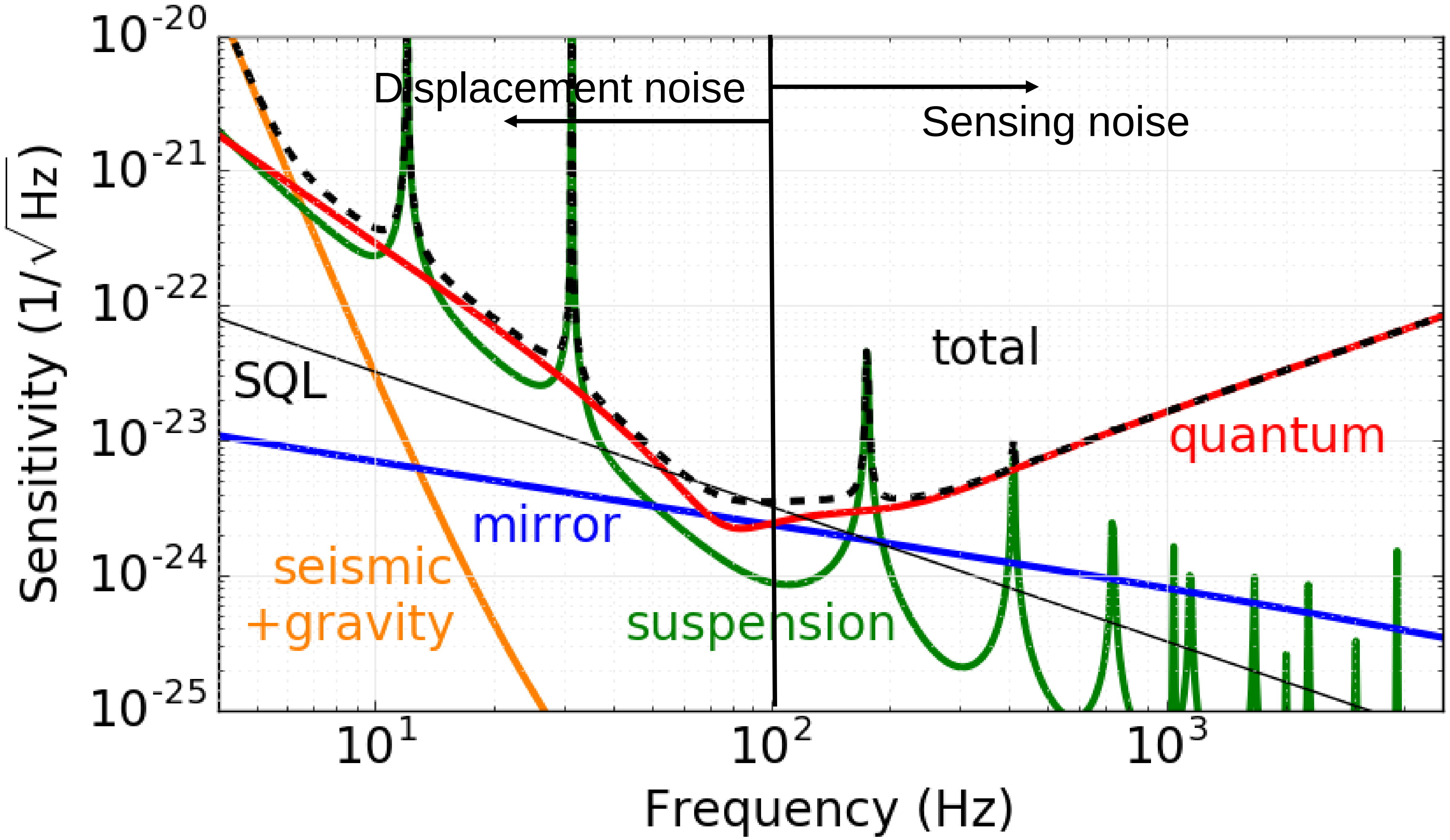

High and low frequency sensitivity is limited by disturbances and sensing noise, respectively

Global network and multi-messenger astronomy

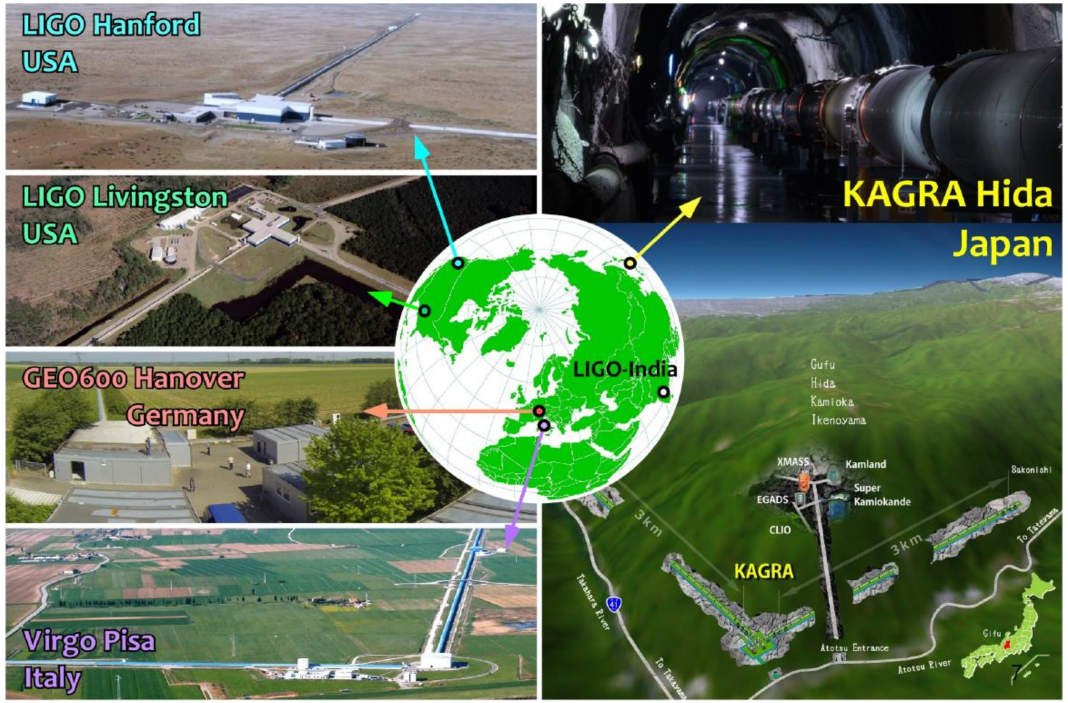

Network duty factor
2023 May 24 15:00 UTC – June 20 23:00 UTC

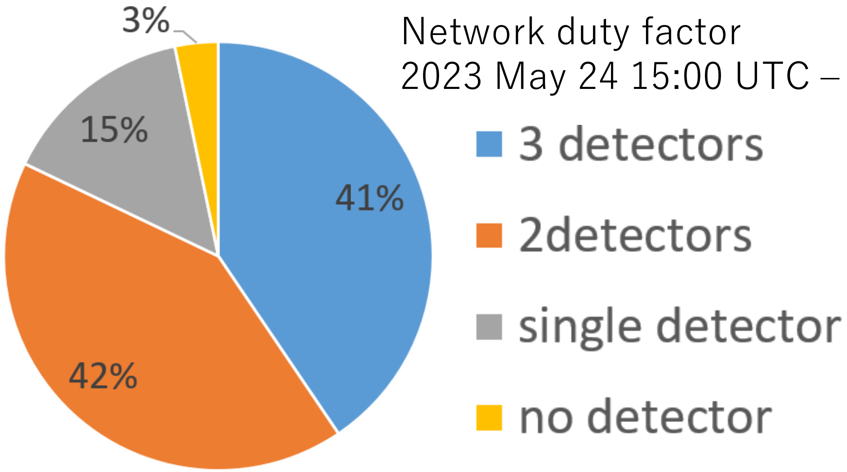

LLO: 82.5%
LHO: 53.1%
KAGRA: 82.4%

- More than 200 candidate events so far.
- One successful follow-up observation: GW170817
  - ➢ GW, short GRB, and afterglow
  - ➢ Counterpart was identified.
  - ➢ Standard siren etc.

- Multiple-detector observation is essential for:
  - ➢ better localization
  - ➢ better observation coincidence
  - ➢ Polarization of GWs

- Increase of the number of detectors are important.

Past observing run

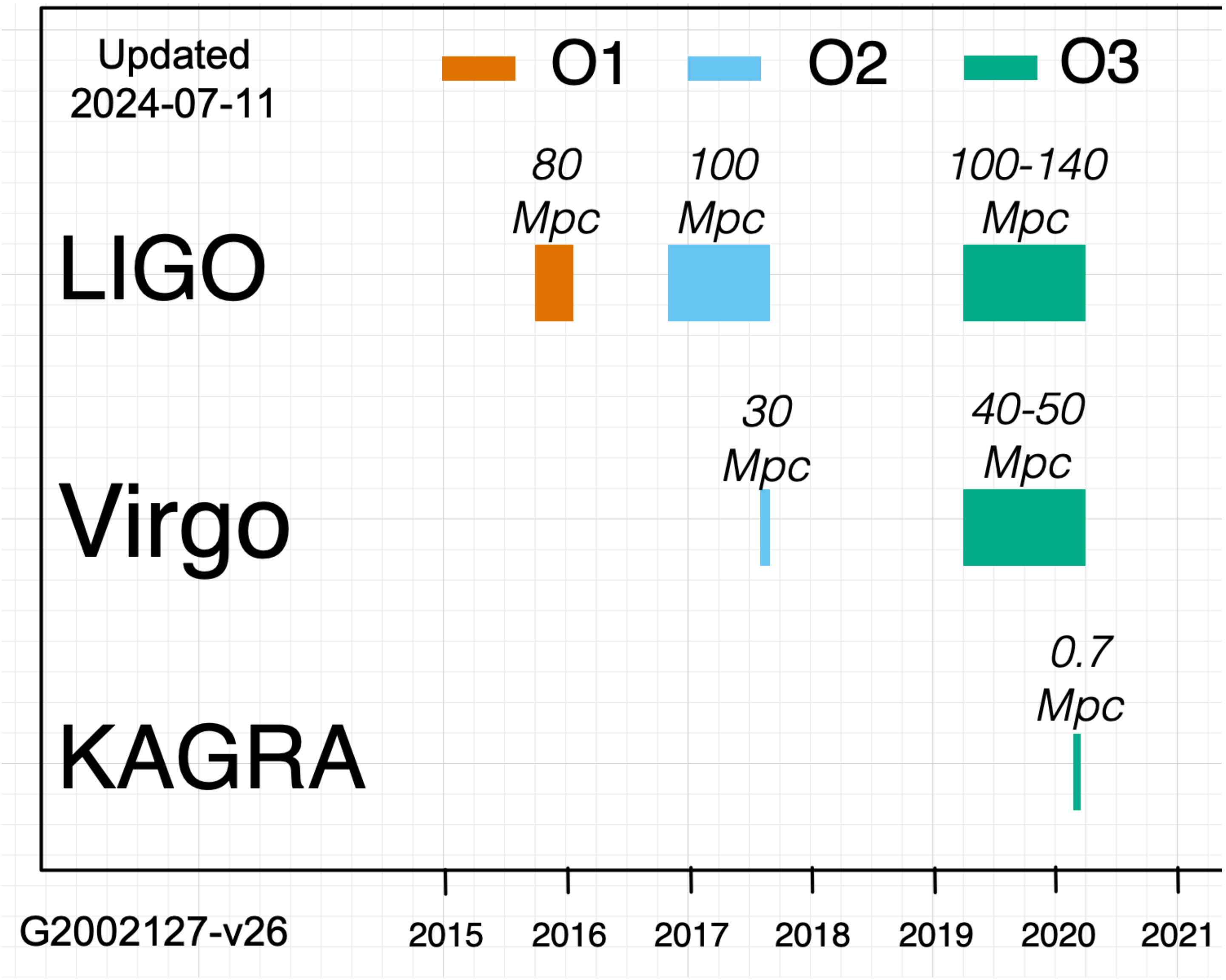

1st Observing Run (O1)
2015 Sep. – 2016 Jan.

- 2 LIGO detectors
- GW150914:
  First detection of BBH merger.

2nd Observing Run (O2)
2016 Nov. – 2017 Aug.

- 2 LIGO and Virgo (in Aug.)
- GW170814:
  First detection with 3 detectors.
- GW170817:
  First detection of BNS coalescence.
  Multi-messenger astronomy

3rd Observing Run (O3):
2019 Apr. – 2020 Mar. (O3a and O3b)

- 2 LIGO and Virgo detectors
- GW200105:
  First detection of NS-BH merger candidate.

2020 Apr. (O3GK)

- KAGRA and GEO600

Current and Future observing Run

4th Observing Run (O4)
2023 May. – 2025 Jun.

- 2 LIGO and KAGRA detectors started O4a run.
- KAGRA stopped O4a to improve sensitivity.
- LIGO continues observing run.
- Virgo joined the observing run from the spring 2024.
- KAGRA plan to start the observing run in spring 2025.

5th Observing Run (O5)

- Starting time has not been decided yet.
- Detail term has also not been decided.

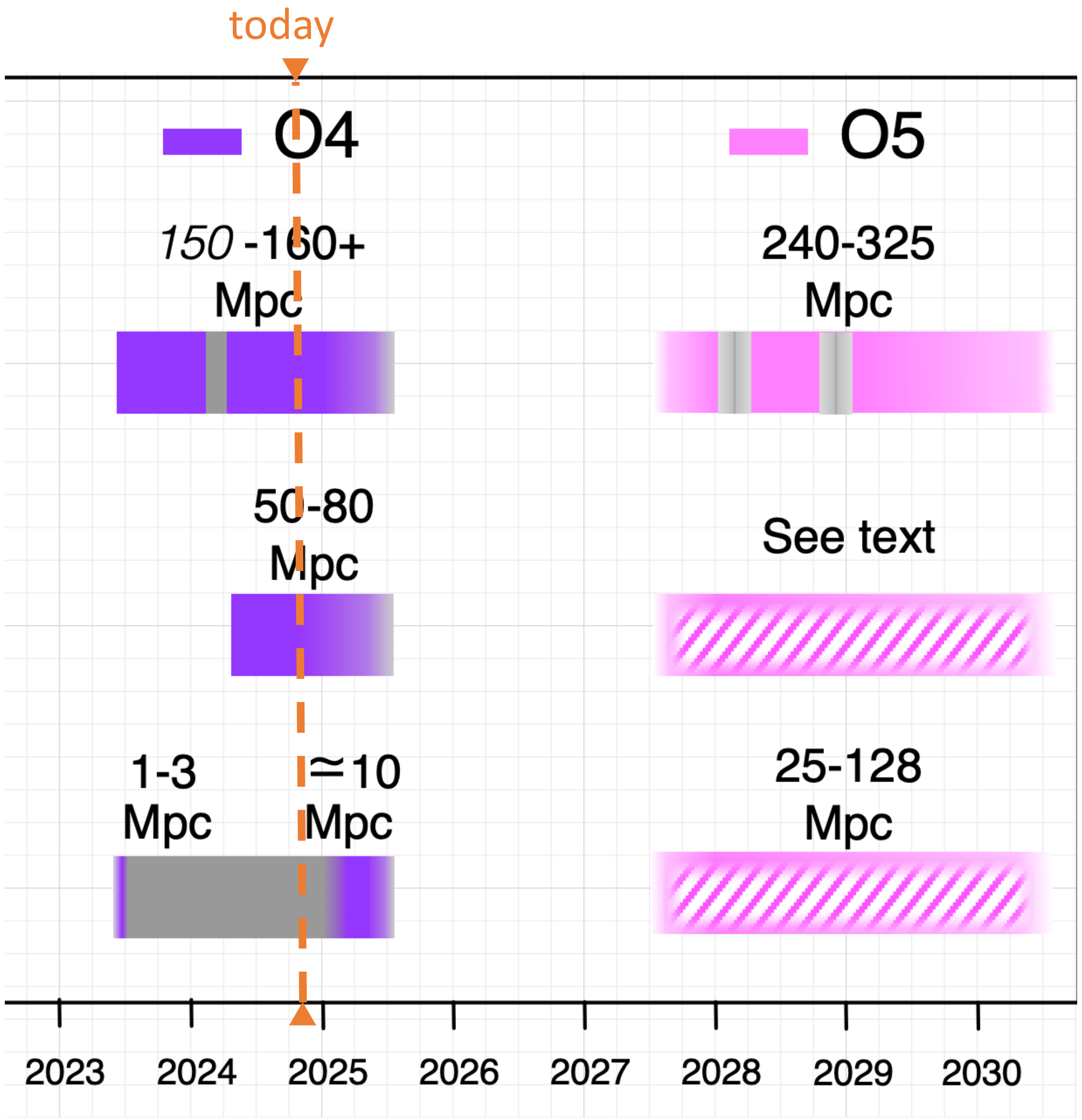

GW detection and candidate so far

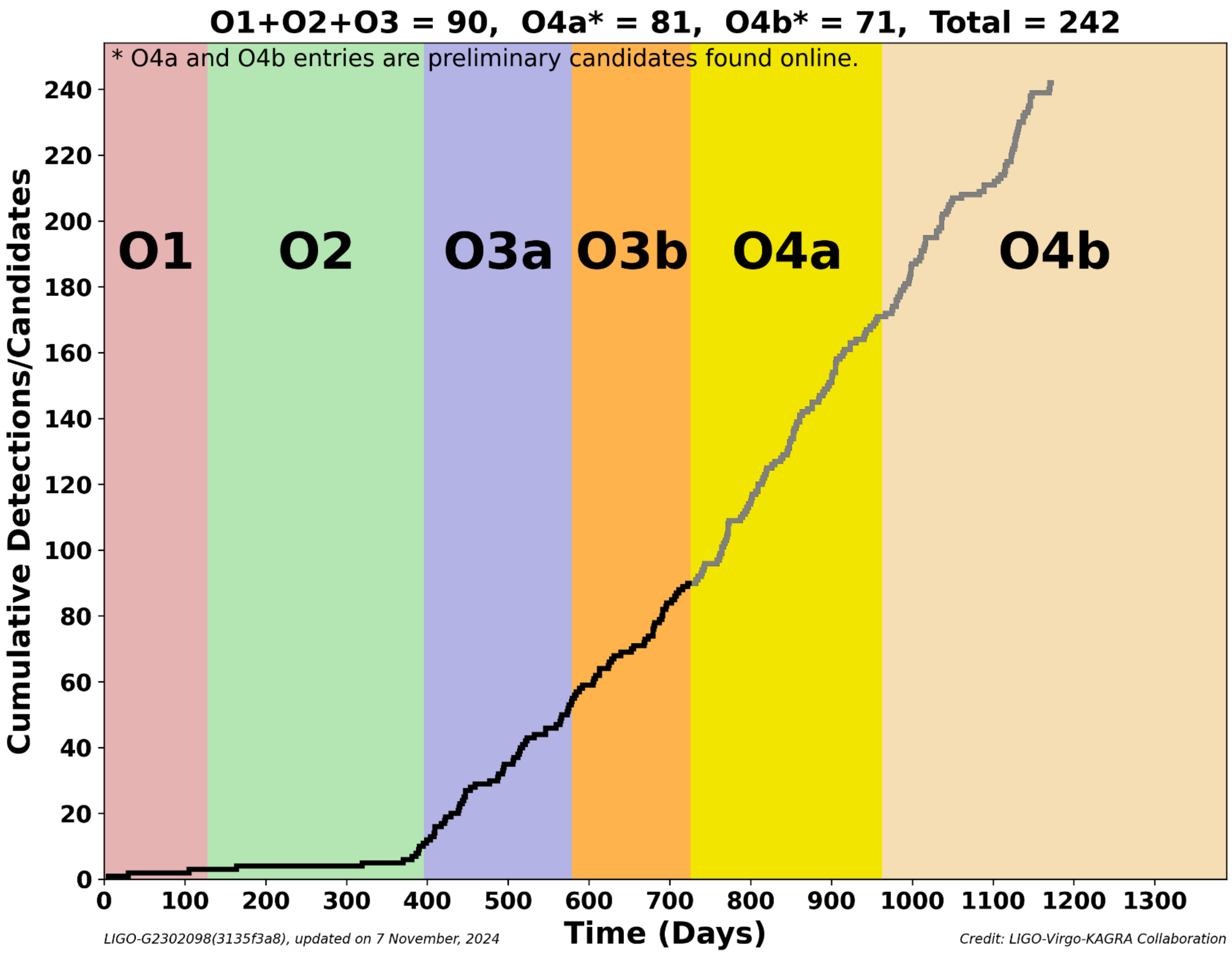

Nov. 7

90 GW events and 152 GW event candidates were observed so far.

Several examples of GW detections

- GW150914: First detection of GW signals from Binary Black Hole (BBH) merger.
  - ➢ Signals are consistent with the merger of 2 BHs with the mass of 36 and 29 solar masses.
- GW170817: First detection of GW signals from Binary Neutron Star (BNS) merger.
  - ➢ Signals are consistent with the mergers of 2 NSs with known NS mass range.
  - ➢ Short Gamma-Ray Burst (SGRB, GRB170817A) was detected 1.7 s after the merger
- GW190425: BNS merger with the heavier mass compared with the galactic BNS
  - ➢ Estimated total mass of the BNS is about 3.3 solar masses, which is greater than galactic BNS mass distribution (less than 3 solar masses).
- GW190521: Heavy BBH merger
  - ➢ One of the primary BHs has a mass of 71-106 solar masses, which is in the mass gap of BHs.
  - ➢ Remnant is an intermediate mass BH with a mass of about 142 solar masses.
- GW190814: BBH merger with high mass ratio
  - ➢ A secondary object has a mass of ~2.6 solar masses, which is in lower mass gap of BHs
- GW200105/ GW200115 : BH-NS merger candidate
  - ➢ Masses of primary and secondary objects are consistent with the NSBH merger.

GW150914

PRL 116, 061102 (2016)

TABLE I. Source parameters for GW150914. We report median values with 90% credible intervals that include statistical errors, and systematic errors from averaging the results of different waveform models. Masses are given in the source frame; to convert to the detector frame multiply by $(1+z)$ [90]. The source redshift assumes standard cosmology [91].

Primary black hole mass	$36^{+5}_{-4} M_\odot$
Secondary black hole mass	$29^{+4}_{-4} M_\odot$
Final black hole mass	$62^{+4}_{-4} M_\odot$
Final black hole spin	$0.67^{+0.05}_{-0.07}$
Luminosity distance	410^{+160}_{-180} Mpc
Source redshift z	$0.09^{+0.03}_{-0.04}$

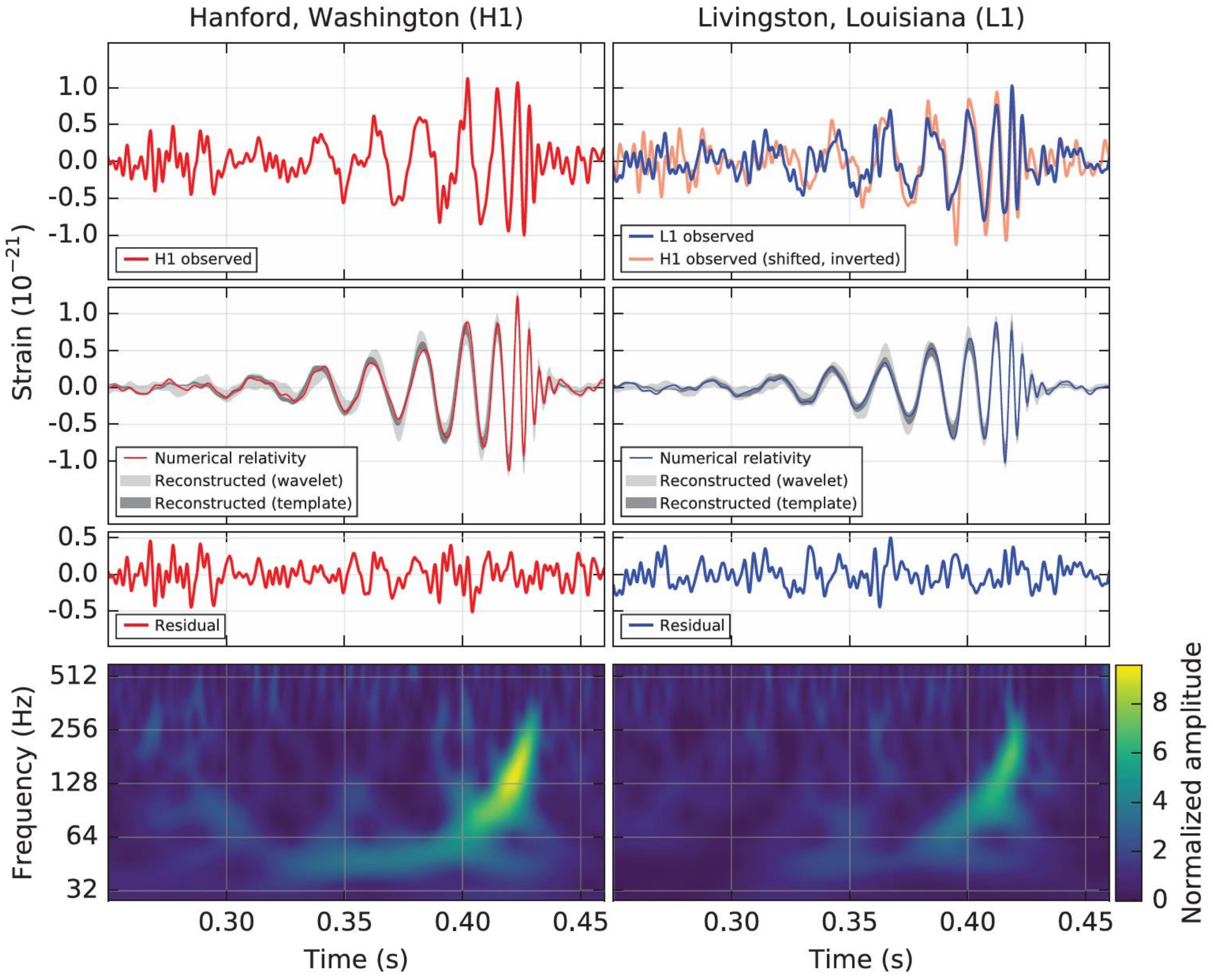

FIG. 1. The gravitational-wave event GW150914 observed by the LIGO Hanford (H1, left column panels) and Livingston (L1, right column panels) detectors. Times are shown relative to September 14, 2015 at 09:50:45 UTC. For visualization, all time series are filtered with a 35–350 Hz bandpass filter to suppress large fluctuations outside the detectors' most sensitive frequency band, and band-reject filters to remove the strong instrumental spectral lines seen in the Fig. 3 spectra. *Top row, left:* H1 strain. *Top row, right:* L1 strain. GW150914 arrived first at L1 and $6.9^{+0.5}_{-0.4}$ ms later at H1; for a visual comparison, the H1 data are also shown, shifted in time by this amount and inverted (to account for the detectors' relative orientations). *Second row:* Gravitational-wave strain projected onto each detector in the 35–350 Hz band. Solid lines show a numerical relativity waveform for a system with parameters consistent with those recovered from GW150914 [37,38] confirmed to 99.9% by an independent calculation based on [15]. Shaded areas show 90% credible regions for two independent waveform reconstructions. One (dark gray) models the signal using binary black hole template waveforms [39]. The other (light gray) does not use an astrophysical model, but instead calculates the strain signal as a linear combination of sine-Gaussian wavelets [40,41]. These reconstructions have a 94% overlap, as shown in [39]. *Third row:* Residuals after subtracting the filtered numerical relativity waveform from the filtered detector time series. *Bottom row:*A time-frequency representation [42] of the strain data, showing the signal frequency increasing over time.

Demonstration of GW detection
Demonstration of BBH system

GW170817

The Astrophysical Journal Letters, 848:L12 (59pp), 2017

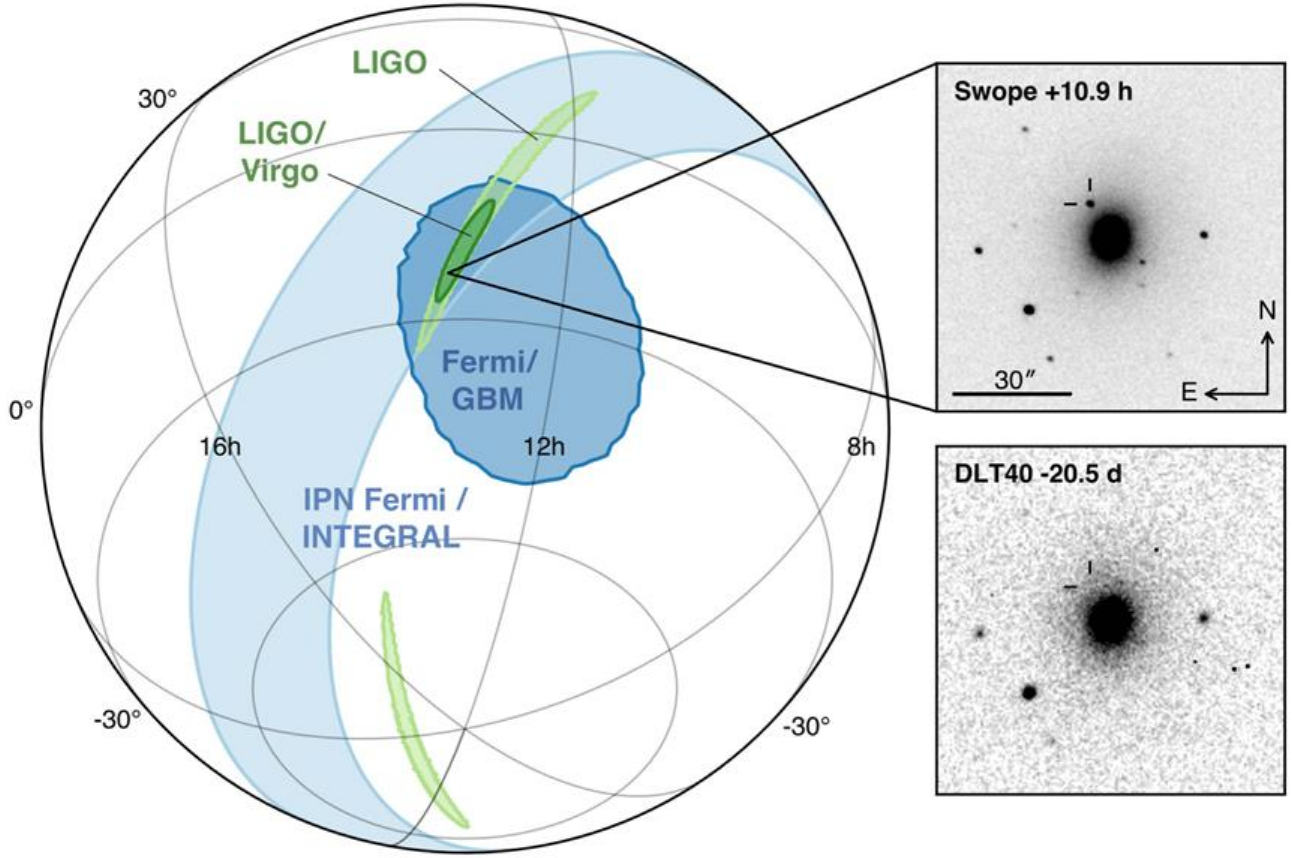

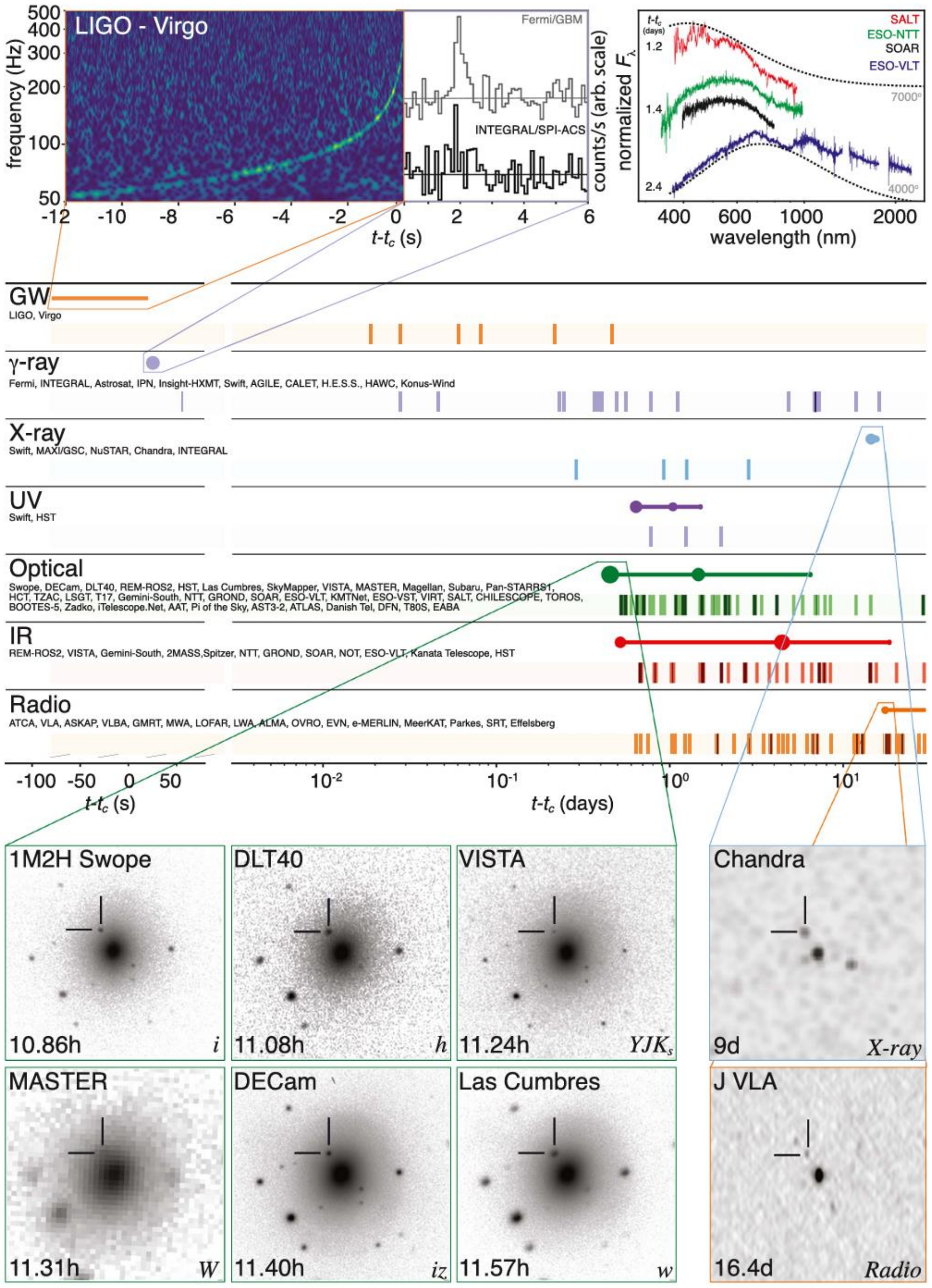

- Origin of SGRB and kilonova
- Constraint to speed of GWs.
- Origin of heavy element
- Standard siren measurement of the Hubble constant

(Nature volume 551, pages85–88 (2017))

GW190425

The Astrophysical Journal Letters, 892:L3 (24pp), 2020

Table 1
Source Properties for GW190425

	Low-spin Prior ($\chi < 0.05$)	High-spin Prior ($\chi < 0.89$)
Primary mass m_1	1.60–1.87 $M_\odot$	1.61–2.52 $M_\odot$
Secondary mass m_2	1.46–1.69 $M_\odot$	1.12–1.68 $M_\odot$
Chirp mass $\mathcal{M}$	$1.44^{+0.02}_{-0.02}$ $M_\odot$	$1.44^{+0.02}_{-0.02}$ $M_\odot$
Detector-frame chirp mass	$1.4868^{+0.0003}_{-0.0003}$ $M_\odot$	$1.4873^{+0.0008}_{-0.0006}$ $M_\odot$
Mass ratio m_2/m_1	0.8 – 1.0	0.4 – 1.0
Total mass $m_{\rm tot}$	$3.3^{+0.1}_{-0.1}$ $M_\odot$	$3.4^{+0.3}_{-0.1} M_\odot$
Effective inspiral spin parameter $\chi_{\rm eff}$	$0.012^{+0.01}_{-0.01}$	$0.058^{+0.11}_{-0.05}$
Luminosity distance $D_{\rm L}$	159^{+69}_{-72} Mpc	159^{+69}_{-71} Mpc
Combined dimensionless tidal deformability $\tilde{\Lambda}$	$\leqslant 600$	$\leqslant 1100$

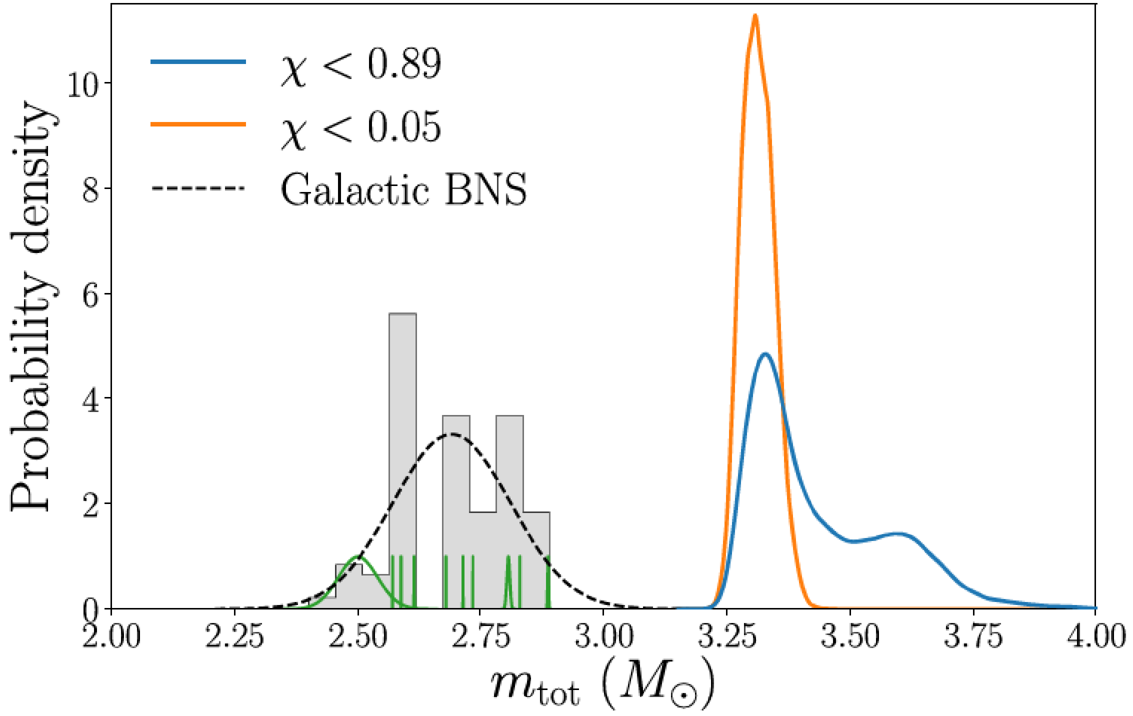

Figure 5. Total system masses for GW190425 under different spin priors, and those for the 10 Galactic BNSs from Farrow et al. (2019) that are expected to merge within a Hubble time. The distribution of the total masses of the latter is shown and fit using a normal distribution shown by the dashed black curve. The green curves are for individual Galactic BNS total mass distributions rescaled to the same ordinate axis height of 1.

- Observing heavier BNS system, which was found in our galaxy.
- Detection with only LLO because LHO was not observing.
- No EM/neutrino counter part.

GW190521

PHYSICAL REVIEW LETTERS 125, 101102 (2020)

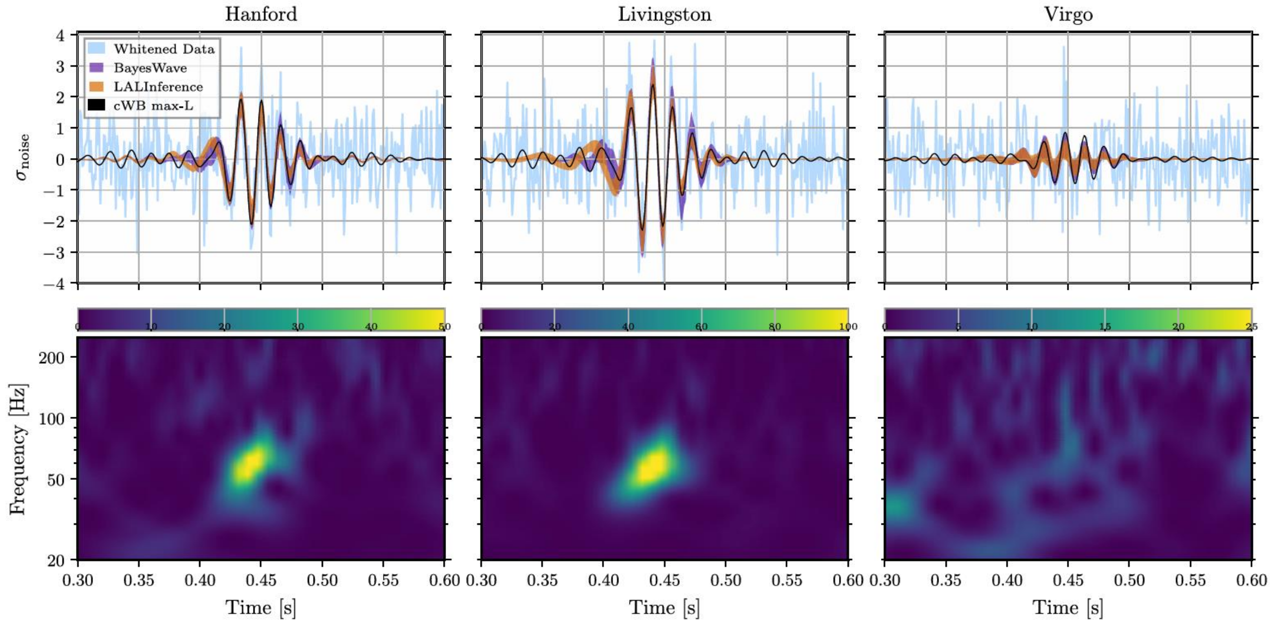

FIG. 1. The GW event GW190521 observed by the LIGO Hanford (left), LIGO Livingston (middle), and Virgo (right) detectors. Times are shown relative to May 21, 2019 at 03:02:29 UTC. The top row displays the time-domain detector data after whitening by each instrument's noise amplitude spectral density (light blue lines); the point estimate waveform from the CWB search [43] (black lines); the 90% credible intervals from the posterior probability density functions of the waveform time series, obtained via Bayesian inference (LALINFERENCE [49]) with the NRSur7dq4 binary BH waveform model [50] (orange bands), and with a generic wavelet model (BayesWave [51], purple bands). The ordinate axes are in units of noise standard deviations. The bottom row displays the time-frequency representation of the whitened data using the Q transform [52].

- Demonstrate BH in heavier mass gap.
- Demonstrate an intermediate mass BH.

TABLE I. Parameters of GW190521 according to the NRSur7dq4 waveform model. We quote median values with 90% credible intervals that include statistical errors.

Parameter	
Primary mass	$85^{+21}_{-14}\ M_\odot$
Secondary mass	$66^{+17}_{-18}\ M_\odot$
Primary spin magnitude	$0.69^{+0.27}_{-0.62}$
Secondary spin magnitude	$0.73^{+0.24}_{-0.64}$
Total mass	$150^{+29}_{-17}\ M_\odot$
Mass ratio ($m_2/m_1 \leq 1$)	$0.79^{+0.19}_{-0.29}$
Effective inspiral spin parameter (χ_{eff})	$0.08^{+0.27}_{-0.36}$
Effective precession spin parameter (χ_{p})	$0.68^{+0.25}_{-0.37}$
Luminosity Distance	$5.3^{+2.4}_{-2.6}$ Gpc
Redshift	$0.82^{+0.28}_{-0.34}$
Final mass	$142^{+28}_{-16}\ M_\odot$
Final spin	$0.72^{+0.09}_{-0.12}$
$P\ (m_1 < 65\ M_\odot)$	0.32%
$\log_{10}$ Bayes factor for orbital precession	$1.06^{+0.06}_{-0.06}$
$\log_{10}$ Bayes factor for nonzero spins	$0.92^{+0.06}_{-0.06}$
$\log_{10}$ Bayes factor for higher harmonics	$-0.38^{+0.06}_{-0.06}$

GW190814

The Astrophysical Journal Letters, 896:L44 (20pp), 2020

Table 1
Source Properties of GW190814: We Report the Median Values Along with the Symmetric 90% Credible Intervals for the SEOBNRV4PHM (EOBNR PHM) and IMRPHENOMPV3HM (PHENOM PHM) Waveform Models

	EOBNR PHM	Phenom PHM	Combined
Primary mass $m_1/M_\odot$	$23.2^{+1.0}_{-0.9}$	$23.2^{+1.3}_{-1.1}$	$23.2^{+1.1}_{-1.0}$
Secondary mass $m_2/M_\odot$	$2.59^{+0.08}_{-0.08}$	$2.58^{+0.09}_{-0.10}$	$2.59^{+0.08}_{-0.09}$
Mass ratio q	$0.112^{+0.008}_{-0.008}$	$0.111^{+0.009}_{-0.010}$	$0.112^{+0.008}_{-0.009}$
Chirp mass $\mathcal{M}/M_\odot$	$6.10^{+0.06}_{-0.05}$	$6.08^{+0.06}_{-0.05}$	$6.09^{+0.06}_{-0.06}$
Total mass $M/M_\odot$	$25.8^{+0.9}_{-0.8}$	$25.8^{+1.2}_{-1.0}$	$25.8^{+1.0}_{-0.9}$
Final mass $M_f/M_\odot$	$25.6^{+1.0}_{-0.8}$	$25.5^{+1.2}_{-1.0}$	$25.6^{+1.1}_{-0.9}$
Upper bound on primary spin magnitude χ_1	0.06	0.08	0.07
Effective inspiral spin parameter $\chi_{\rm eff}$	$0.001^{+0.059}_{-0.056}$	$-0.005^{+0.061}_{-0.065}$	$-0.002^{+0.060}_{-0.061}$
Upper bound on effective precession parameter χ_p	0.07	0.07	0.07
Final spin χ_f	$0.28^{+0.02}_{-0.02}$	$0.28^{+0.02}_{-0.03}$	$0.28^{+0.02}_{-0.02}$
Luminosity distance D_L/Mpc	235^{+40}_{-45}	249^{+39}_{-43}	241^{+41}_{-45}
Source redshift z	$0.051^{+0.008}_{-0.009}$	$0.054^{+0.008}_{-0.009}$	$0.053^{+0.009}_{-0.010}$
Inclination angle Θ/rad	$0.9^{+0.3}_{-0.2}$	$0.8^{+0.2}_{-0.2}$	$0.8^{+0.3}_{-0.2}$
Signal-to-noise ratio in LIGO Hanford ρ_H	$10.6^{+0.1}_{-0.1}$	$10.7^{+0.1}_{-0.2}$	$10.7^{+0.1}_{-0.2}$
Signal-to-noise ratio in LIGO Livingston ρ_L	$22.21^{+0.09}_{-0.15}$	$22.16^{+0.09}_{-0.17}$	$22.18^{+0.10}_{-0.17}$
Signal-to-noise ratio in Virgo ρ_V	$4.3^{+0.2}_{-0.5}$	$4.1^{+0.2}_{-0.6}$	$4.2^{+0.2}_{-0.6}$
Network Signal-to-noise ratio ρ_{HLV}	$25.0^{+0.1}_{-0.2}$	$24.9^{+0.1}_{-0.2}$	$25.0^{+0.1}_{-0.2}$

Note. The primary spin magnitude and the effective precession is given as the 90% upper limit. The inclination angle is folded to $[0, \pi/2]$. The last column is the result of combining the posteriors of each model with equal weight. The sky location of GW190814 is shown in Figure 2.

- Demonstrate objects in lower mass gap.
- No electromagnetic counter part.
- Consistent with GR prediction and higher-multipole emission is confirmed with high coinfidence

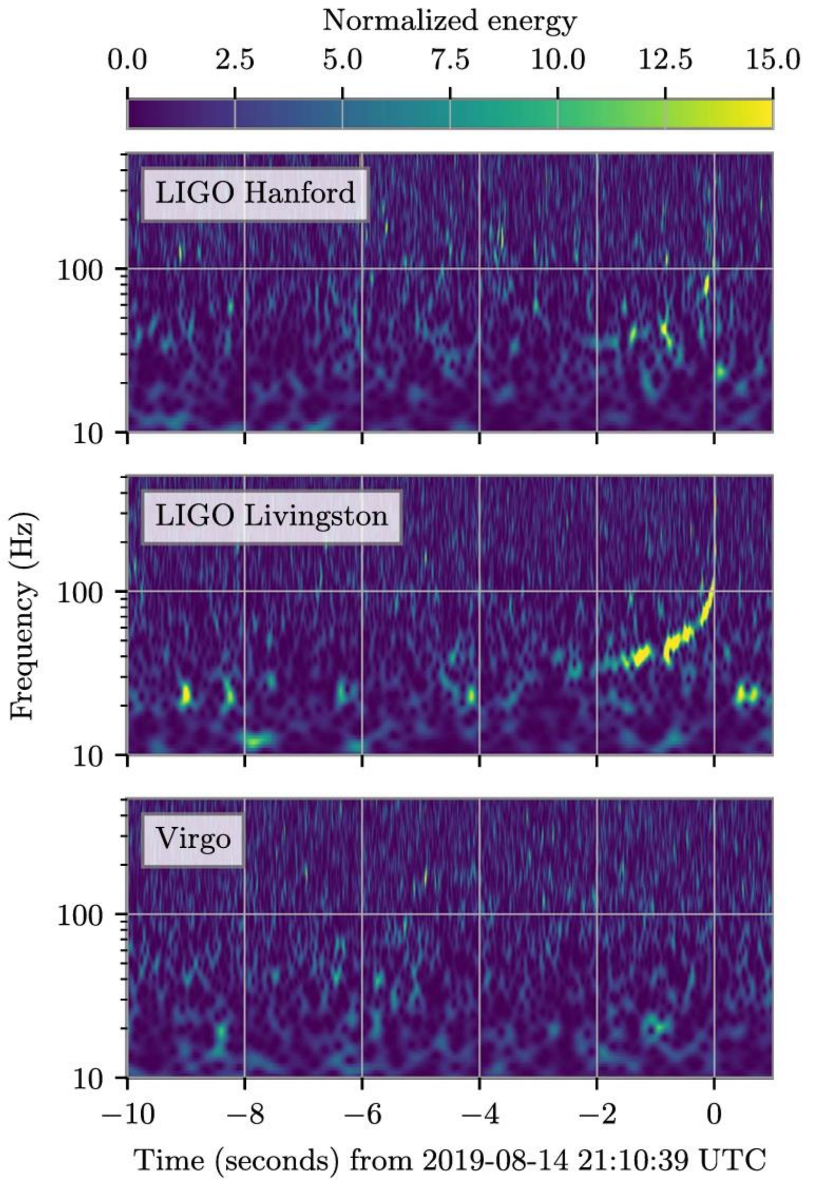

Figure 1. Time–frequency representations (Chatterji et al. 2004) of data containing GW190814, observed by LIGO Hanford (top), LIGO Livingston (middle), and Virgo (bottom). Times are shown relative to 2019 August 14, 21:10:39 UTC. Each detector's data are whitened by their respective noise amplitude spectral density and a Q-transform is calculated. The colorbar displays the normalized energy reported by the Q-transform at each frequency. These plots are not used in our detection procedure and are for visualization purposes only.

GW200105

The Astrophysical Journal Letters, 915:L5 (24pp), 2021

Table 2
Source Properties of GW200105 and GW200115

	GW200105		GW200115	
	Low Spin ($\chi_2 < 0.05$)	High Spin ($\chi_2 < 0.99$)	Low Spin ($\chi_2 < 0.05$)	High Spin ($\chi_2 < 0.99$)
Primary mass $m_1/M_\odot$	$8.9^{+1.1}_{-1.3}$	$8.9^{+1.2}_{-1.5}$	$5.9^{+1.4}_{-2.1}$	$5.7^{+1.8}_{-2.1}$
Secondary mass $m_2/M_\odot$	$1.9^{+0.2}_{-0.2}$	$1.9^{+0.3}_{-0.2}$	$1.4^{+0.6}_{-0.2}$	$1.5^{+0.7}_{-0.3}$
Mass ratio q	$0.21^{+0.06}_{-0.04}$	$0.22^{+0.08}_{-0.04}$	$0.24^{+0.31}_{-0.08}$	$0.26^{+0.35}_{-0.10}$
Total mass $M/M_\odot$	$10.8^{+0.9}_{-1.0}$	$10.9^{+1.1}_{-1.2}$	$7.3^{+1.2}_{-1.5}$	$7.1^{+1.5}_{-1.4}$
Chirp mass $\mathcal{M}/M_\odot$	$3.41^{+0.08}_{-0.07}$	$3.41^{+0.08}_{-0.07}$	$2.42^{+0.05}_{-0.07}$	$2.42^{+0.05}_{-0.07}$
Detector-frame chirp mass $(1+z)\mathcal{M}/M_\odot$	$3.619^{+0.006}_{-0.006}$	$3.619^{+0.007}_{-0.008}$	$2.580^{+0.006}_{-0.007}$	$2.579^{+0.007}_{-0.007}$
Primary spin magnitude χ_1	$0.09^{+0.18}_{-0.08}$	$0.08^{+0.22}_{-0.08}$	$0.31^{+0.52}_{-0.29}$	$0.33^{+0.48}_{-0.29}$
Effective inspiral spin parameter $\chi_{\rm eff}$	$-0.01^{+0.08}_{-0.12}$	$-0.01^{+0.11}_{-0.15}$	$-0.14^{+0.17}_{-0.34}$	$-0.19^{+0.23}_{-0.35}$
Effective precession spin parameter χ_p	$0.07^{+0.15}_{-0.06}$	$0.09^{+0.14}_{-0.07}$	$0.19^{+0.28}_{-0.17}$	$0.21^{+0.30}_{-0.17}$
Luminosity distance $D_{\rm L}$/Mpc	280^{+110}_{-110}	280^{+110}_{-110}	310^{+150}_{-110}	300^{+150}_{-100}
Source redshift z	$0.06^{+0.02}_{-0.02}$	$0.06^{+0.02}_{-0.02}$	$0.07^{+0.03}_{-0.02}$	$0.07^{+0.03}_{-0.02}$

Note. We report the median values with 90% credible intervals. Parameter estimates are obtained using the Combined PHM samples.

- Signals are consistent with NS-BH merger.
- No electromagnetic counter part
- No tidal deformation information.

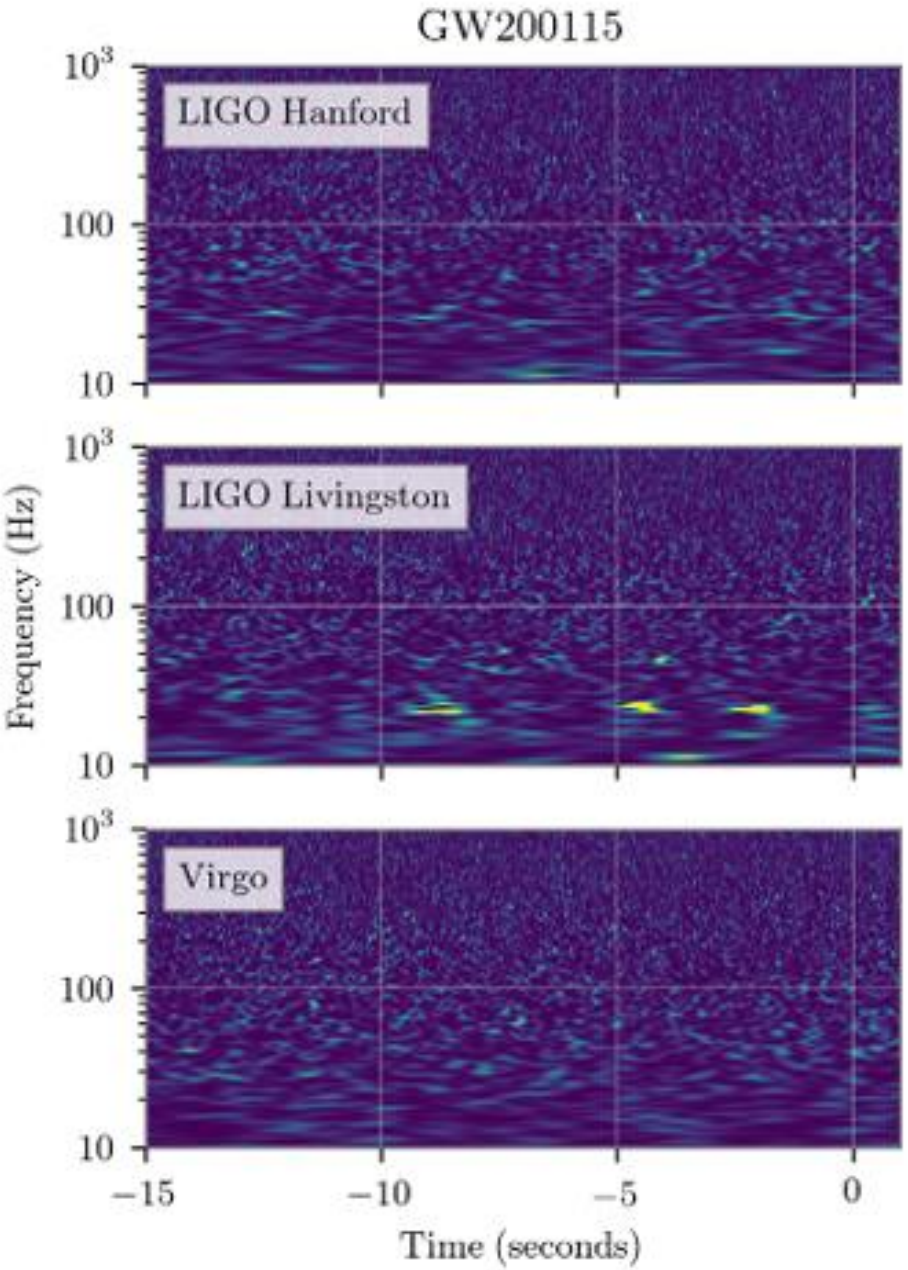

Several examples of other science with GW detectors

PHYSICAL REVIEW D **105,** 063030 (2022)
PHYSICAL REVIEW D **109,** 089902(E) (2024)

Constraints on dark photon dark matter using data from LIGO's and Virgo's third observing run

R. Abbott *et al.*[*]
(LIGO Scientific Collaboration, Virgo Collaboration, and KAGRA Collaboration)

(Received 27 May 2021; accepted 8 March 2022; published 31 March 2022)

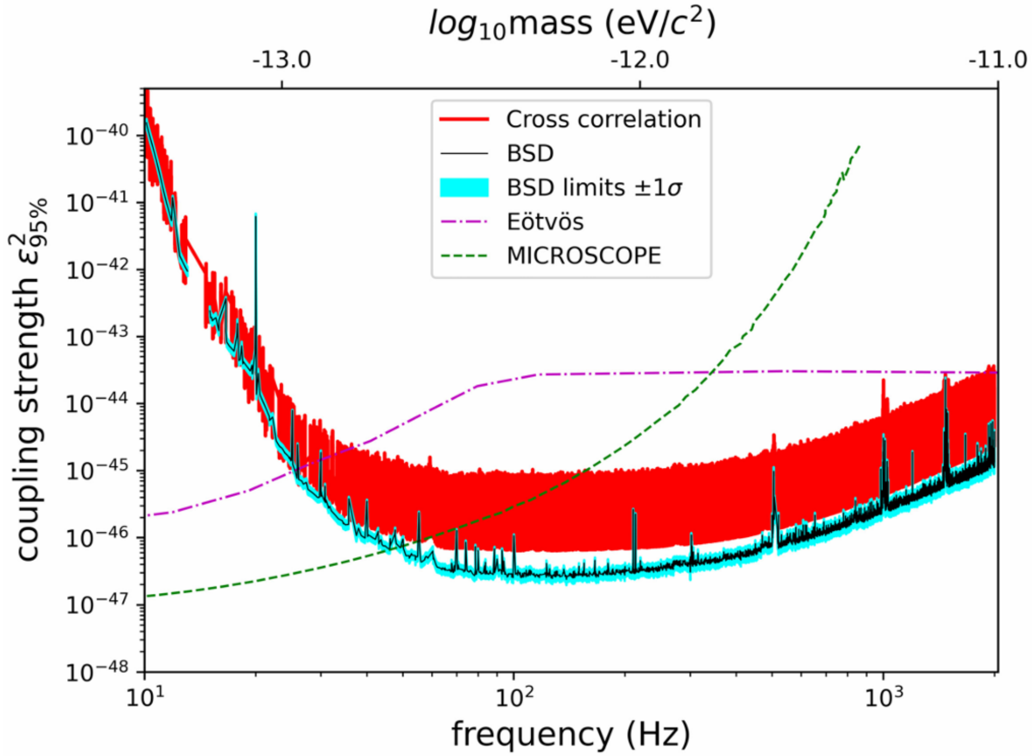

Tightest bound for dark photon coupling strength around 10^{-12} eV/c^2

PHYSICAL REVIEW D **110,** 042001 (2024)

Ultralight vector dark matter search using data from the KAGRA O3GK run

A. G. Abac *et al.*[*]
(LIGO Scientific, Virgo, and KAGRA Collaborations)

(Received 12 March 2024; accepted 8 July 2024; published 22 August 2024)

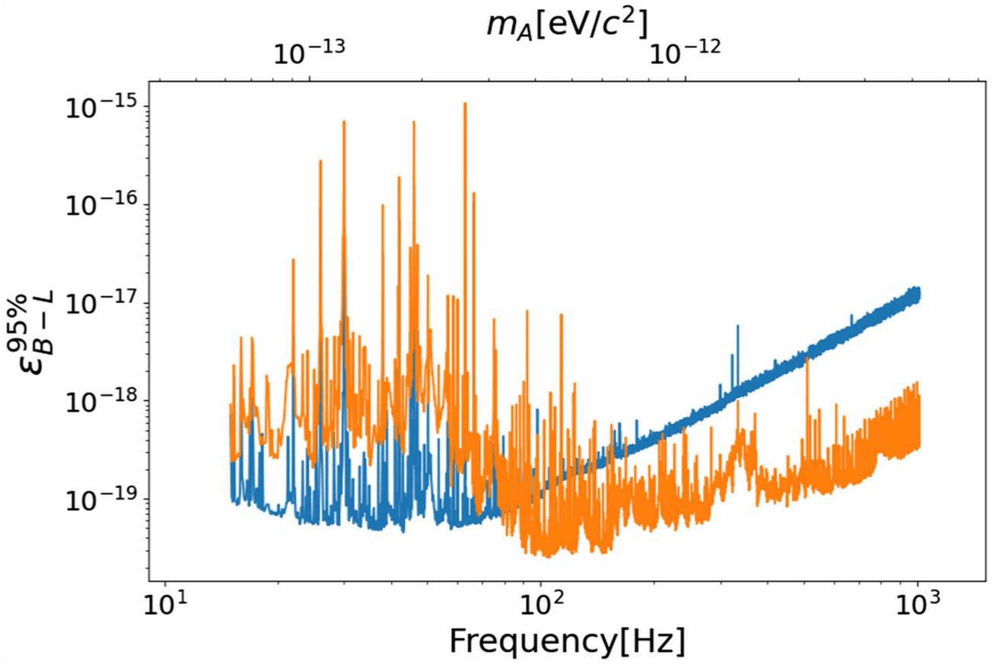

FIG. 6. 95% upper limit on the $B - L$ gauge coupling constant derived from MICH data (blue line) and PRCL data (orange line). Many narrow peaks observed in lower mass range are due to unknown line artifacts in the lower frequency range.

KAGRA

An interferometric gravitational-wave detector with 3km arm in Hida city.

Two unique key features:

- Using underground site → Reduction of seismic noise
- Cooling sapphire mirrors → Reduction of thermal noise

KAGRA joined the beginning of O4a (2023 May 25 – 2023 June 21 JST)

Configuration

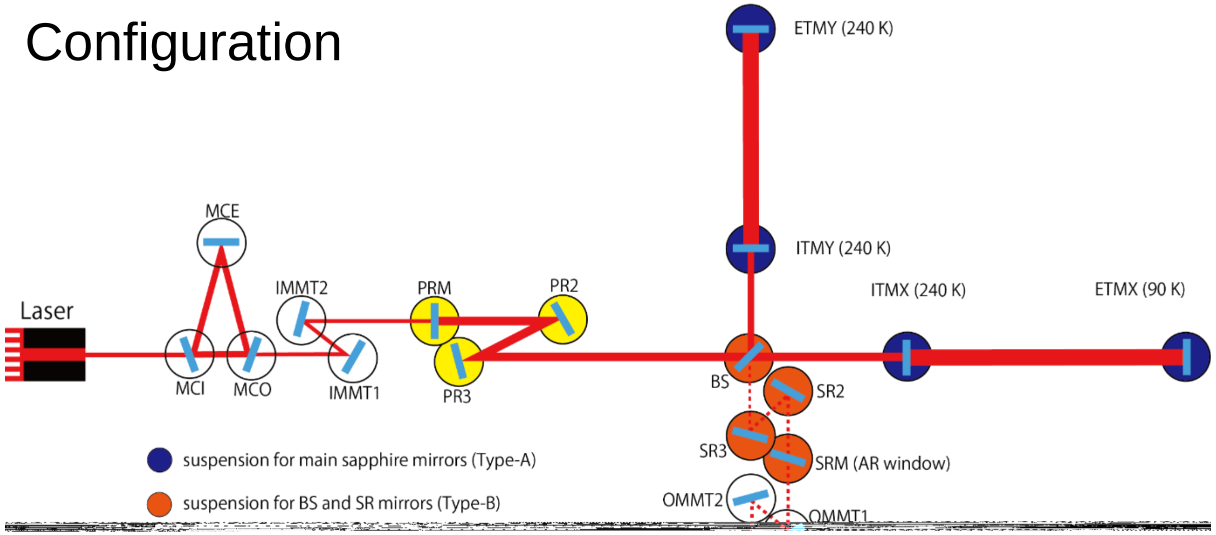

Sensitivity and duty factor during O4a

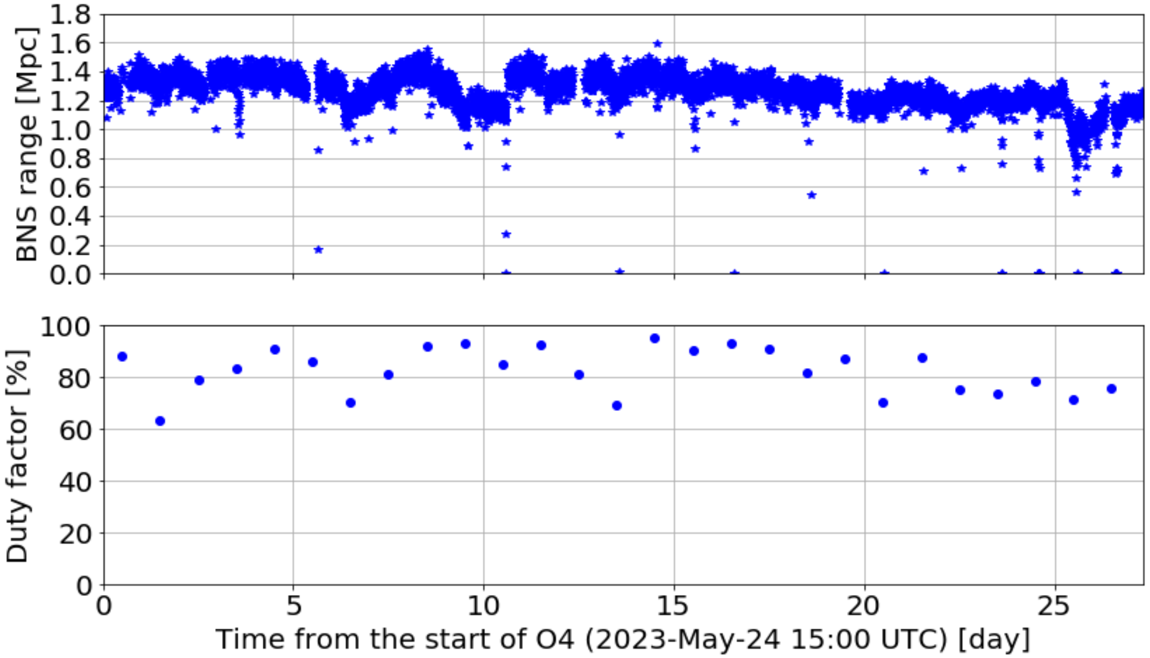

Noise budget during O4a

Low frequency :
- Local control noise
- Auxiliary control noise

Middle frequency :
- Thermal noise
- Acoustic noise
- PD dark noise

High frequency :
- Laser frequency
- Shot noise
- PD dark noise

The detector was well characterized.

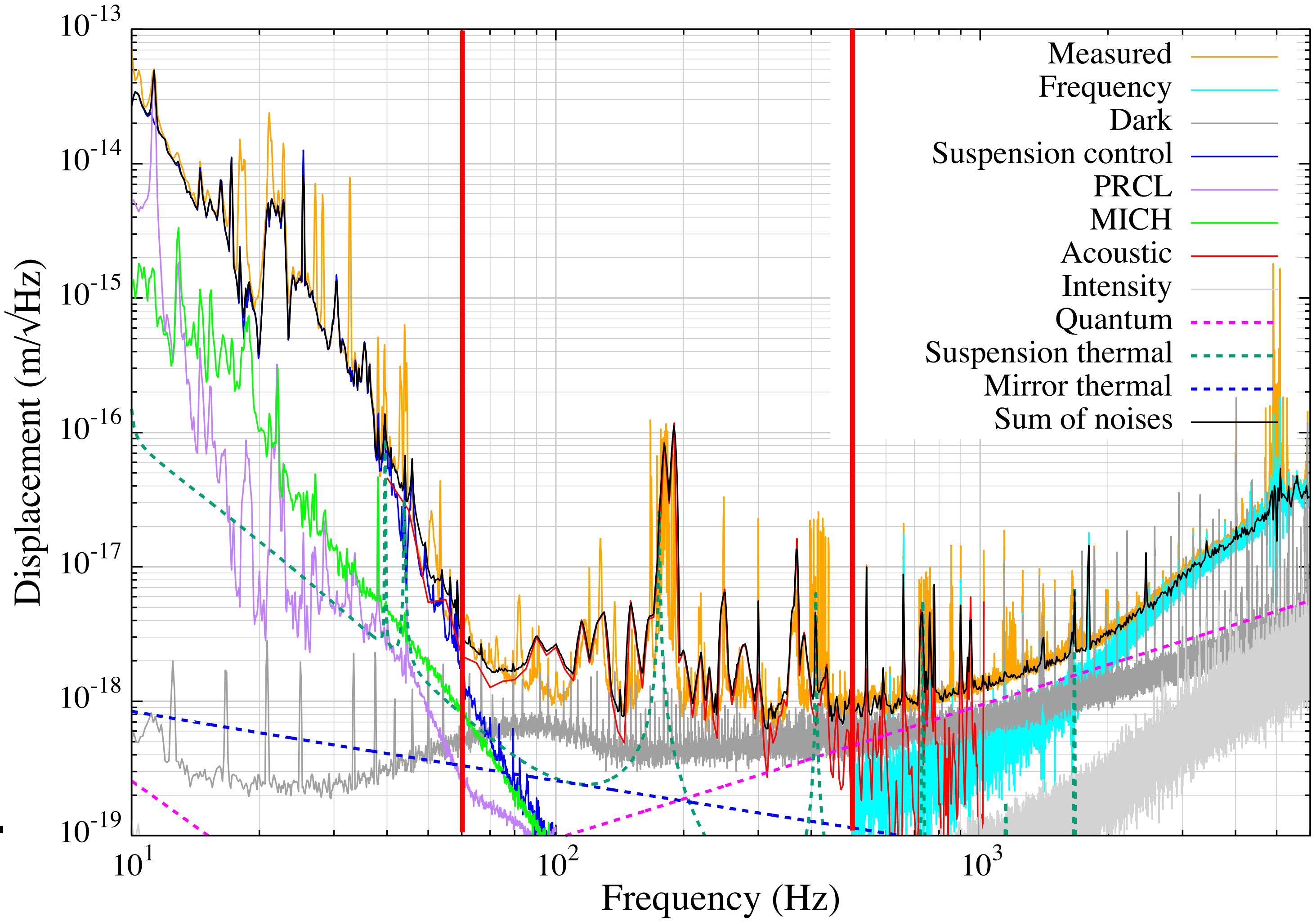

We initially planed to rejoin O4b from the spring in 2024, though ⋯

2024 Noto earthquake

The large earthquake was occurred at Noto and hit the KAGRA site.

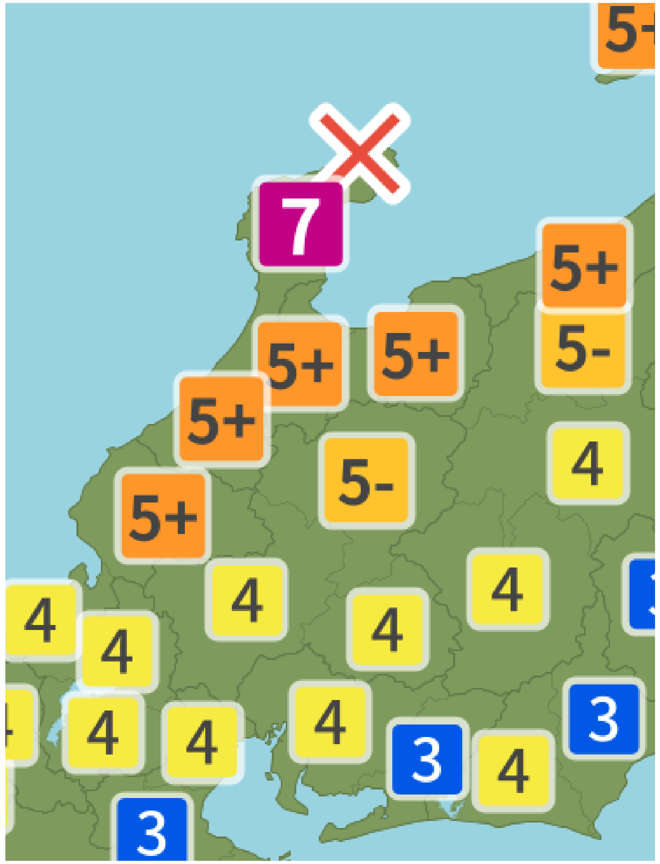

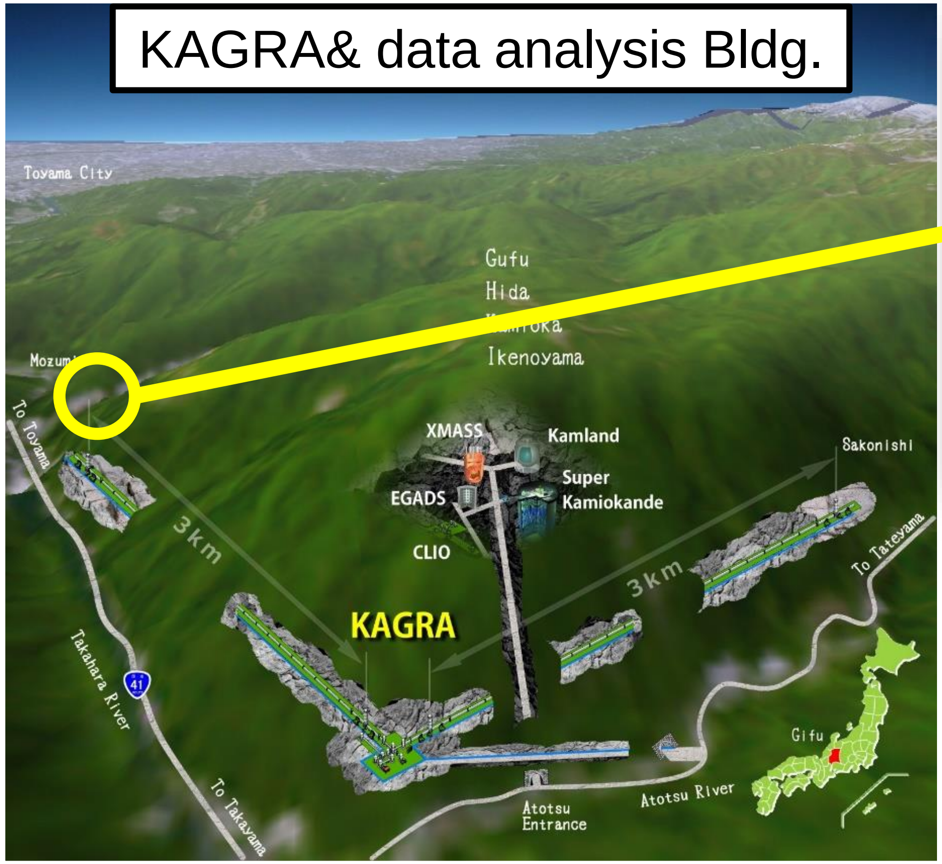

Seismic intensity level of 5: the largest earthquake in the past 100 years.

Crustal deformation in order of cm was observed around KAGRA site.

Damage due to the Noto earthquake

Some failure in suspensions:

- Type-A suspension:
  - Magnets are fallen off
- Type-Bp suspensions:
  - Magnets are fallen off
  - Mirror was tilted and went to the out of adjustable range
- Type-C suspensions:
  - Magnets are fallen off
  - Mirror was tilted and went to the out of adjustable range

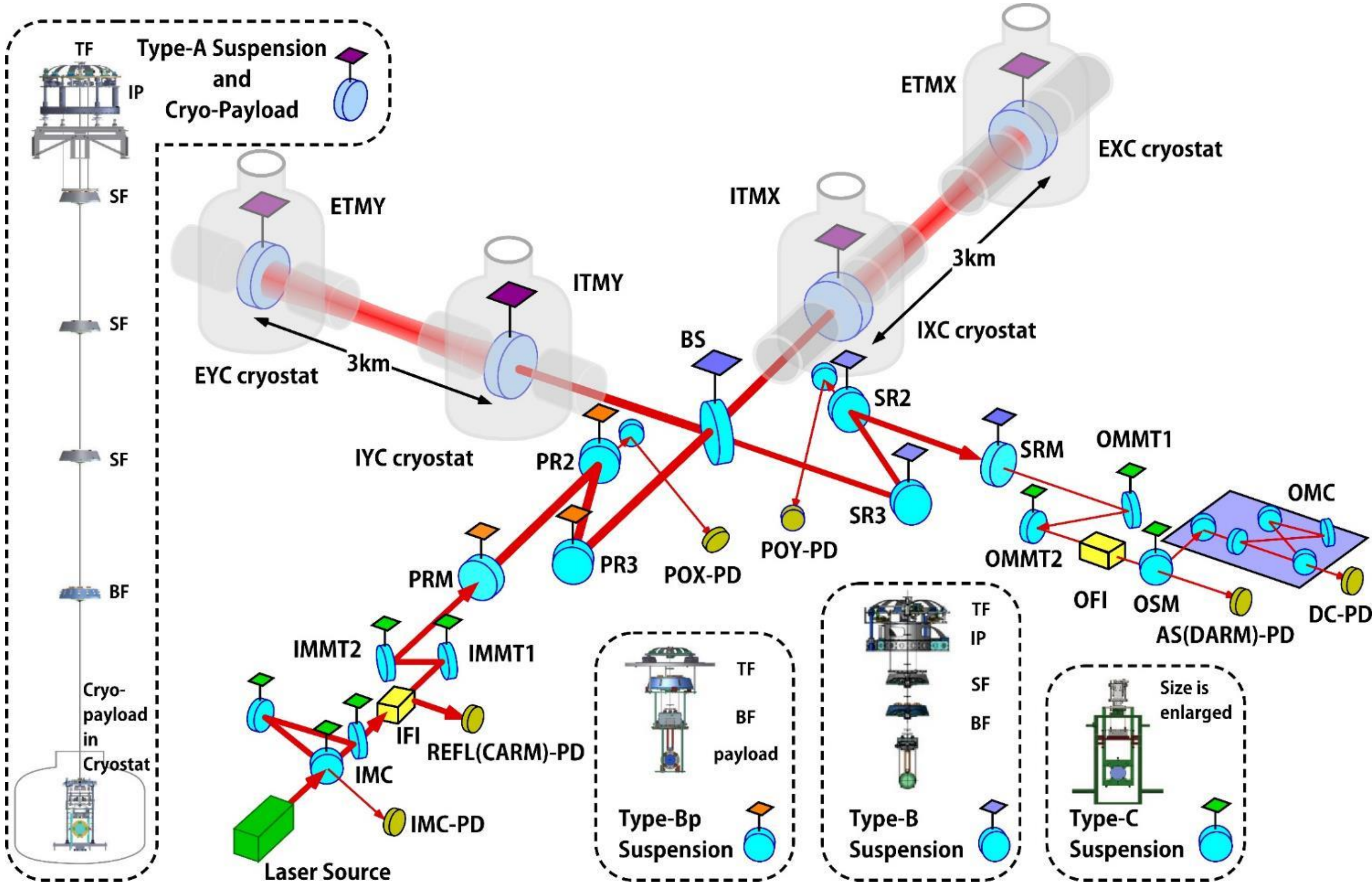

It took more than 2 months to confirm which suspensions were damaged.
All vacuum were vented except for arm tubes.
Since all mirrors were cooled down, it took a long time to open all vacuum chambers.

Schedule after the earthquake

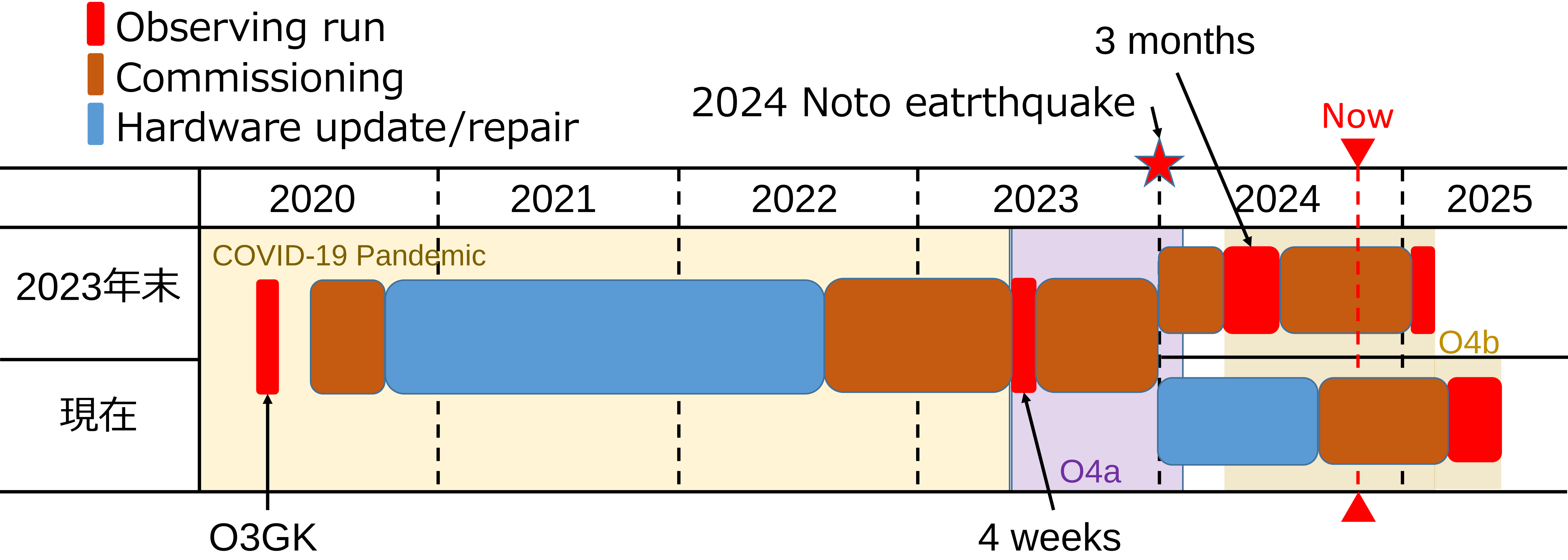

Initial plan: Observing run for 3 months in spring 2024 and in 2025 with better sensitivity

→ We gave up observing run in 2024 and concentrated the recovery of KAGRA. Rejoining O4 in spring 2025 with better sensitivity

Current recovery status

Recovery of suspensions：

- All magnets rebounding and rough mirror alignment (June)

Recovery of vacuum：

- Vacuum evacuation of all vauum tanks (July)
- Passing vacuum leak test for all tanks (September)

Recovery of the interferometer：

- Observation mode at room temperature (October)

Cooling was started in late October and continued.

Fully cooled down in the early next year.

Toward O4b

- Already reduced noise：
  - ➢ Suspension local control noise：1/10
  - ➢ PD dark noise: below shot noise

- Future noise reduction：

  High power operation：
  - ➢ Auxiliary control noise：1/10
  - ➢ Quantum shot noise：1/3

  Cooling：
  - ➢ Thermal noise：1/5

  Control/hardware update：
  - ➢ Frequency noise：～1/2
  - ➢ Acoustic noise：～1/20

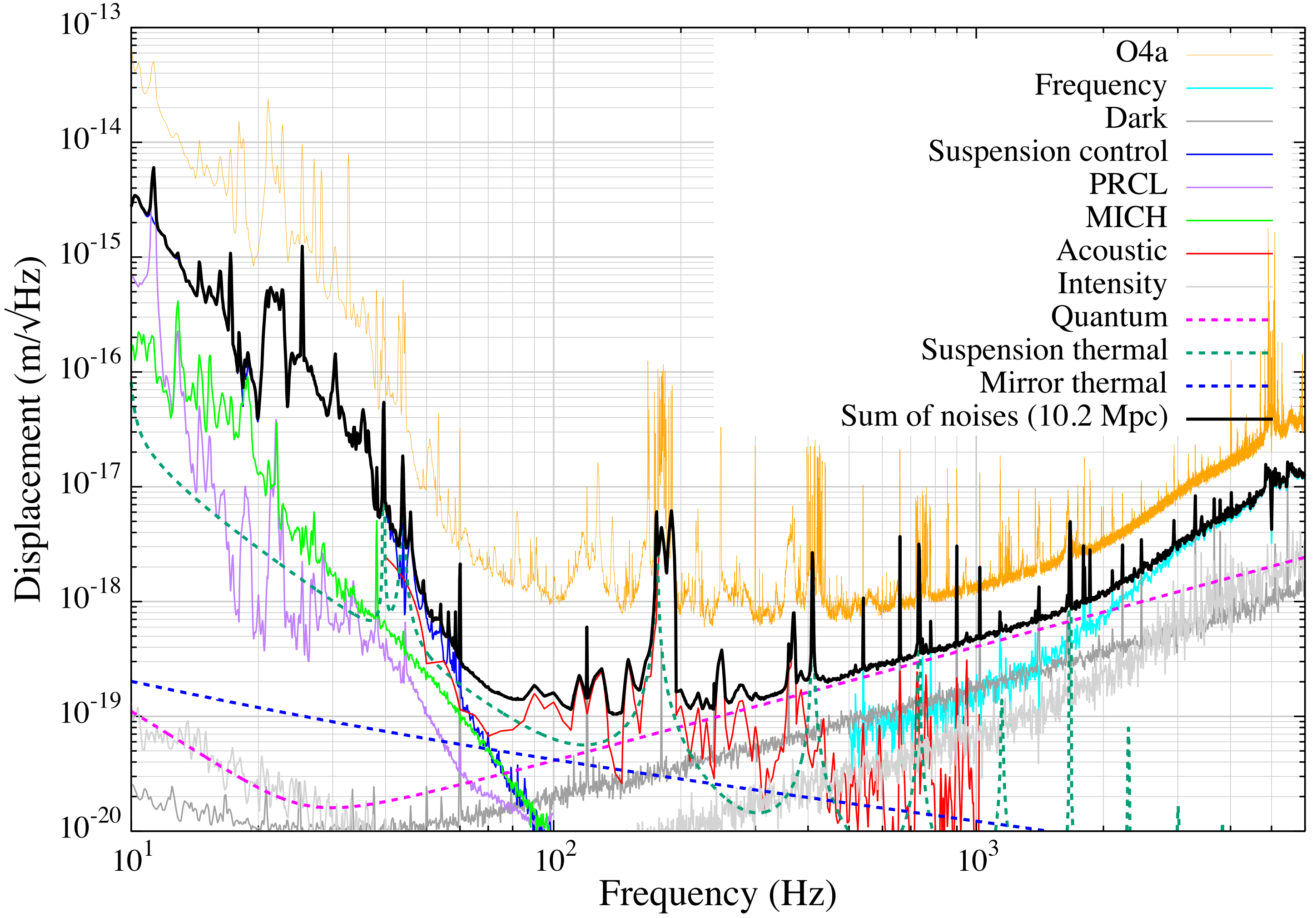

Aim to rejoin O4 in the spring 2025 with the sensitivity close to 10 Mpc

Acoustic noise reduction

Acoustic noise around signals detection port (OMC) was performed.

Repair of OMC stack

before

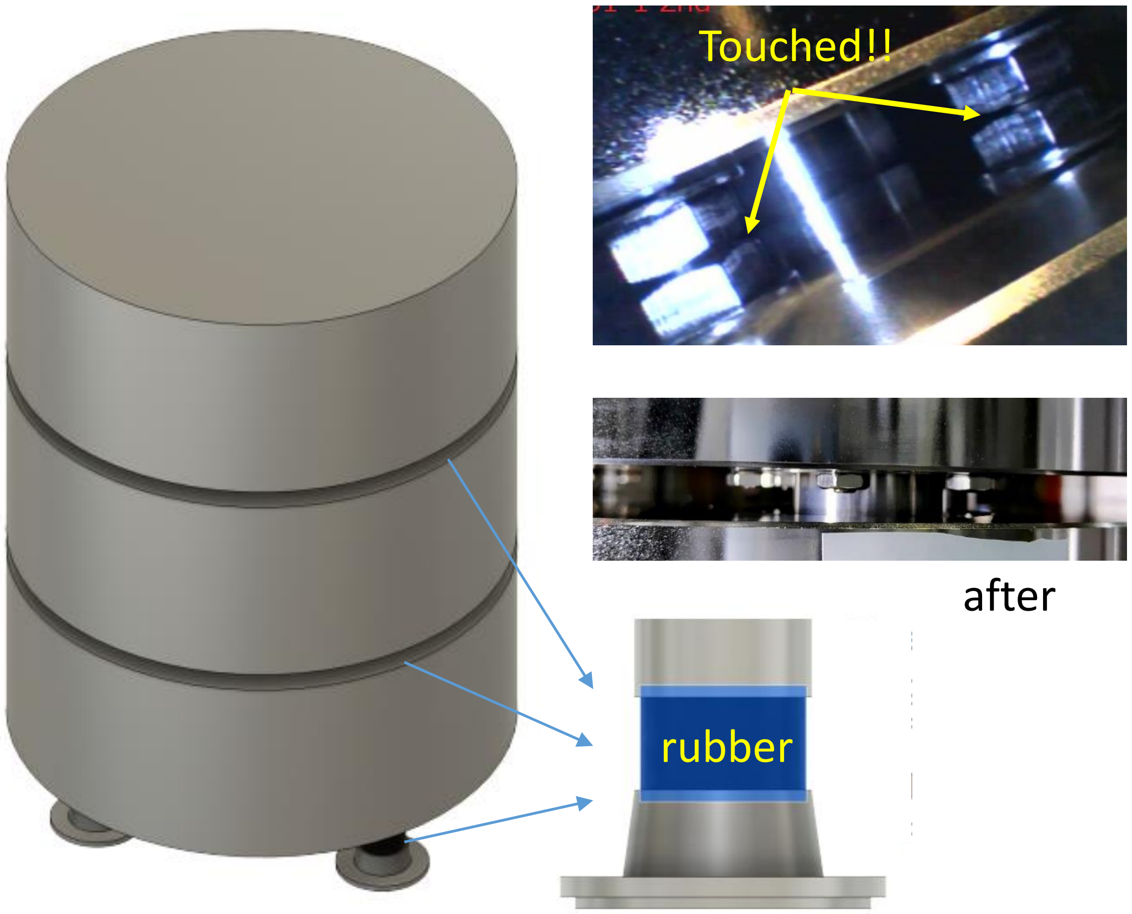

Installation of magnet dampers

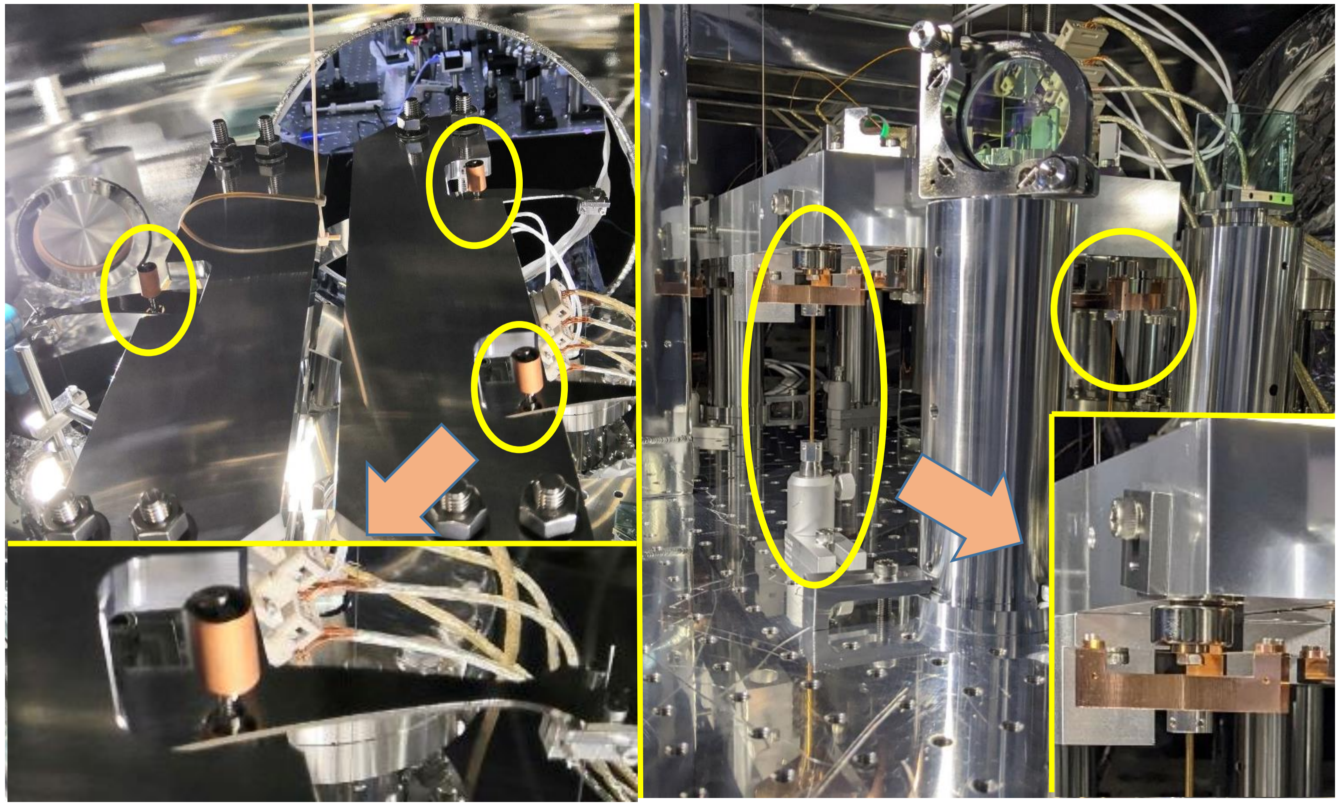

Damper for blade spring

Damper for pendulum

Latest sensitivity

Configuration: Room-temperature PRFPMI with 1.3W injection

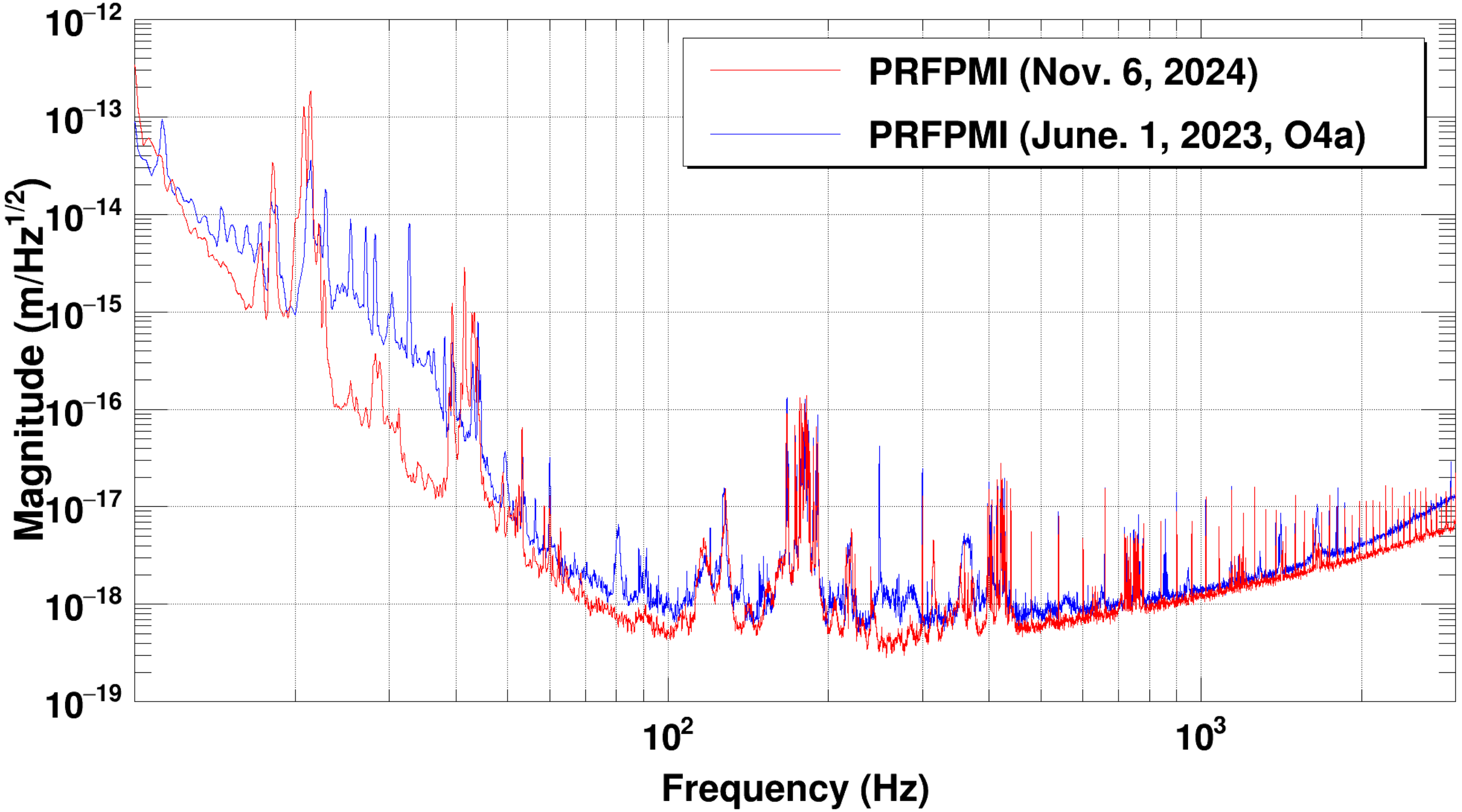

Some updates to the hardware and controls of the interferometer have improved sensitivity across all frequency bands as well as restoring the interferometer.
Continue to commission the interferometer to achieve our target sensitivity for O4b.

Beyond O4

Further sensitivity enhancement by following actions:

- Increase laser power
  - ➢ Preparation of high power laser is ongoing (40W max → 60W max)

- Achieve more advanced interferometer configuration
  - ➢ As like LIGO, RSE technique will be utilized o enhance high frequency sensitivity.

- Installing new mirrors as input mirrors
  - ➢ Making better quality mirror is now preparing for O5

- Update vibration isolation systems
  - ➢ Some mechanical update for suspensions and vibration isolation stack is discussed.

- Installing PDs inside the vacuum.
  - ➢ Design of vacuum compatible PD housing are started.

and so on.

Summary

- O4 observing run has started since 24 of May 2023 and will end in June 2025.

- Many GW sources have been found, and the number of interesting observations will increase with the number of events found.

- KAGRA joined O4 from May 25 2023 to June 21 2023 (JST).
  - ➢ Sensitivity (BNS range) was about 1.3 Mpc.
  - ➢ Duty factor was about 82%.

- Noto earthquake hit KAGR site and causes significant damages to KAGRA, especially suspensions.

- Recovery is still ongoing and we aim to restart the observing run with LIGO and Virgo in 2025 with the sensitivity as better as possible.

- We also proceed some upgrades beyond O4 to further sensitivity enhancement in O5.